Numerical and experimental validation of the applicability of active-DTS experiments to estimate thermal conductivity and groundwater flux in porous media

Nataline Simon, Olivier Bour, Nicolas Lavenant, Gilles Porel, Benoît Nauleau,

Behzad Pouladi, Laurent Longuevergne, Alain Crave

HAL Id: insu-03048099

https://insu.hal.science/insu-03048099

Submitted on 13 Jan 2021

Water Resources Research

Key Points:
- Numerical and experimental validation of two methods to interpret active-Distributed Temperature Sensing (DTS) experiments in sediments
- Determination of thermal conductivity and groundwater flux with low uncertainties
- Definition of the applicability, range of measurements, and limits of active-DTS experiments

Correspondence to:

N. Simon and O. Bour
nataline.simon@univ-rennes1.fr;
olivier.bour@univ-rennes1.fr

Numerical and Experimental Validation of the Applicability of Active-DTS Experiments to Estimate Thermal Conductivity and Groundwater Flux in Porous Media

N. Simon[1] , O. Bour[1], N. Lavenant[1], G. Porel[2] , B. Nauleau[2], B. Pouladi[1], L. Longuevergne[1] , and A. Crave[1]

[1]Univ Rennes, CNRS, Géosciences Rennes – UMR 6118, Rennes, France, [2]Department of Earth Sciences, IC2MP UMR 7285, Université de Poitiers, CNRS, HydrASA, Poitiers, France

Abstract Groundwater flow depends on the heterogeneity of hydraulic properties whose field characterization is challenging. Recently developed active-Distributed Temperature Sensing (DTS) experiments offer the possibility to directly measure groundwater fluxes resulting from heterogeneous flow fields. Here, based on fundamental principles and numerical simulations, two interpretation methods of active-DTS experiments are proposed to estimate both the porous media thermal conductivities and the groundwater fluxes in sediments. These methods rely on the interpretation of the temperature increase measured along a single heated fiber-optic (FO) cable and consider heat transfer processes occurring both through the FO cable itself and through the porous media. The first method relies on the Moving Instantaneous Line Source model that reproduces the temperature increase and provides estimates of thermal conductivity and groundwater flux as well as an evaluation of the temperature rise due to the FO cable. The second method, based on the graphical identification of three characteristic times, provides complementary estimates of flux, fully independent of the effect of the FO cable. Sandbox experiments provide an experimental validation of the interpretation methods, demonstrate the excellent accuracy of groundwater flux estimates (<5%), and highlight the complementarity of both methods. Active-DTS experiments allow investigating groundwater fluxes over a large range spanning $1 \times 10^{-6} - 5 \times 10^{-2}$ m/s, depending on the duration of the experiment. Considering the applicability of active-DTS experiments in different contexts, we propose a general experimental framework for the application of both interpretation methods in the field, making active-DTS field experiments especially promising for many subsurface applications.

1. Introduction

In groundwater hydrology, the characterization of the distribution of groundwater flow within the critical zone received considerable attention in the last decades (Freeze & Cherry, 1979). Our ability to quantify groundwater flow greatly controls our ability to characterize aquifers, predict contaminant transport, and understand biogeochemical reactions and processes occurring in the subsurface (Kalbus et al., 2009; Poeter & Gaylord, 1990). Groundwater flow at interfaces such as recharge and discharge areas also plays a key role in the preservation of groundwater-dependent ecosystems (Kalbus et al., 2006; Sophocleous, 2002). The quantification of groundwater fluxes is also particularly relevant for geothermal energy since they control heat exchange and storage capacities (Diao et al., 2004). Similarly, the characterization of seepage through dams, dikes, and reservoirs is also critical for geotechnical engineering (Foster et al., 2000).

The spatial distribution of groundwater fluxes is largely driven by subsurface heterogeneities. Thus, in past decades, the characterization of the distribution of groundwater fluxes and their quantification relied on the capacity of characterizing and modeling the spatial variability of hydraulic conductivities (de Marsily, 1976). Considering the challenge in characterizing the field variability of hydraulic properties, the use of heat as a tracer has been widely developed and applied to characterize flow in aquifers or at interfaces such as the hyporheic zone (Anderson, 2005; Kurylyk & Irvine, 2019; Kurylyk et al., 2019; Rau et al., 2014). Indeed, the heat propagation is particularly sensitive to flow variations because thermal properties are much less variable than hydraulic conductivity (Anderson, 2005; Mao et al., 2013). Thus, the thermal conductivity

ranges between 0.9 and 4 W/m/K for sedimentary aquifers (Stauffer et al., 2013) while hydraulic conductivity can vary over 12 order of magnitude (Freeze & Cherry, 1979).

Fiber-Optic-Distributed Temperature Sensing (FO-DTS) technology provides continuous temperature records through space and time along fiber-optic (FO) cables at high spatial and temporal resolutions (Habel et al., 2009; SEAFOM, 2010; Smolen & van der Spek, 2003; Tyler et al., 2009; Ukil et al., 2012). The best performing DTS units available (e.g., Silixa Ultima) can provide temperature measurements every second at a 0.125-m sample spacing. Accuracy of temperature measurements and effective spatial resolution depends not only on the performance of the DTS units but also on integration time, FO cable selection, and experimental conditions in the field (Simon et al., 2020). Many applications in hydrologic sciences demonstrated the potential of the tool to characterize water movements and distribution in the subsurface (Selker et al., 2006a, 2006b; Shanafield et al., 2018), especially since the development of active-DTS methods (Bense et al., 2016). Active-DTS methods continuously monitor temperature changes, induced by a heat source and measured along a FO cable. Early applications in open boreholes demonstrated the capability of heat tracer tests to quantify borehole flows (Banks et al., 2014; Leaf et al., 2012; Liu et al., 2013; Read et al., 2015). Contrary to passive-DTS methods that require measuring natural thermal anomalies or natural temperature fluctuations over time to characterize groundwater flows (Anderson, 2005), active-DTS methods are more sensitive to flow and allow investigating flow variations independently of temperature anomalies.

Among active-DTS methods, some authors proposed to monitor the difference of temperature measured between an electrically heated and a nonheated FO cable, which is directly dependent on fluxes (Bense et al., 2016; Read et al., 2014; Sayde et al., 2015). This approach offered the possibility to determine flow velocity distribution all along the FO cable and to quantify fluxes at unprecedented spatial and temporal resolutions. Then, considering the need to characterize flow under a natural gradient without the effect of the borehole (Pehme et al., 2010), further developments focused on deploying active-DTS methods in direct contact with the rock matrix. Active-DTS experiments have thus been conducted in sealed boreholes (Coleman et al., 2015; Maldaner et al., 2019; Munn et al., 2020; F. Selker & J. S. Selker, 2018) and other promising studies proposed the direct deployment of FO cables vertically into unconsolidated sedimentary aquifers using direct-push equipment (Bakker et al., 2015; des Tombe et al., 2019). Concurrently, active-DTS methods were largely developed and applied in unsaturated soils, offering the possibility of estimating the soil water content and thermal properties (Benitez-Buelga et al., 2014; He, Dyck, Horton, Li, et al., 2018; He, Dyck, Horton, Ren, et al., 2018; Sayde et al, 2010, 2014; Weiss, 2003; Wu et al., 2019) or conducting distributed thermal response test for geothermal energy applications (Vélez Márquez et al., 2018; Zhang et al., 2020).

When heating is applied in direct contact with a saturated porous media, the thermal response, namely the elevation of temperature measured along the cable during heating periods, depends on thermal processes through the porous media and thus on water fluxes that dissipate heat through advection. Different approaches have been proposed to interpret this thermal response, such as numerical models (Coleman et al., 2015; Maldaner et al., 2019) and empirical or analytical solutions (Aufleger et al., 2007; Bakx et al., 2019; Maldaner et al., 2019; Perzlmaier et al., 2004). However, the required parameter calibration often makes the application of models difficult in different contexts. Bakker et al. (2015) and des Tombe et al. (2019) have recently proposed the use of analytical solutions, initially developed by Carslaw and Jaeger (1959), to efficiently estimate the distribution of fluxes along the FO cable. These solutions explicitly take into account conduction and advection processes occurring in saturated porous media. However, these applications did not consider the possible spatial variations of the thermal conductivity of sediments. Moreover, since their setup uses a heating cable combined with a separate FO cable used to monitor temperature at a given distance, their analytical solution cannot therefore be applied directly when the same cable is used both as a heat source and to monitor the temperature (Del Val, 2020).

Although previous studies showed the link between groundwater flow and heat dissipation, most applications still depend on a calibration process or involve data uncertainties that preclude the generalization or full validation of active-DTS experiments applied to saturated sediments. To summarize, the use of active-DTS methods to quantify groundwater fluxes in the subsurface would require (i) a general interpretation method that can be easily applied and that takes into account the spatial distribution of the thermal conductivities of sediments, (ii) a validation of the methodology with independent experimental data, and

(iii) a clear discussion about the applicability of the method in the field considering both the range of fluxes that can be measured and the limits of the method.

These are the aims of the present study. In the following, we first present the theoretical background required to interpret active-DTS experiments before presenting the numerical model used to simulate active-DTS experiments in porous media as well as the experiments achieved in the sandbox. Then, numerical simulations results provide an improved understanding of thermal processes controlling the temperature increase. Two interpretation methods are then proposed to interpret the temperature increase measured along a single heated FO cable during active-DTS experiments, providing an estimate of the spatial distribution of both groundwater fluxes and thermal conductivities at an unprecedented uncertainty level. These interpretation methods are first tested by numerical simulations before being experimentally validated. Finally, we discuss the applicability of active-DTS experiments by defining the limitations, range, and uncertainties of measurements. This study offers the possibility of generalizing the application of active-DTS experiments in the field, for a wide range of contexts.

2. Materials and Methods

2.1. Theoretical Background

2.1.1. Heat Transfer Through Porous Media

To quantify groundwater fluxes, we propose deploying a heat source within a porous media and monitoring the surrounding temperature evolution through an active heat tracer experiment using FO-DTS technology. The cable is heated electrically through its steel armoring while the elevation in temperature is continuously monitored using the fiber optic inside the cable. Therefore, a single FO cable is used to measure the surrounding temperature and as a heat source, as applied in some previous studies (Bakx et al., 2019; Bense et al., 2016; Read et al., 2014; F. Selker & J. S. Selker, 2018; Simon et al., 2020).

In this configuration, the temperature increase measured during an active-DTS experiment should be controlled by heat transfer processes occurring in the porous medium. Within a saturated porous medium, heat is transferred by two main mechanisms: advection, which corresponds to the heat transferred by flowing groundwater; and conduction, which corresponds to the molecular diffusion of thermal energy (Anderson, 2005). Without any flow, heat transfer should occur only by conduction and a gradual and continuous increase of temperature is therefore expected. If water flows through the porous medium, advection should partly control the thermal response by dissipating the heat produced by the heat source. The higher the water flow velocity, the lower should be the temperature increase. Note that free thermal convection in the porous media is considered here negligible, which is one of the assumptions required applying the following analytical solutions.

The transport of heat in saturated porous media by conduction and advection is described by the following heat transport equation (Carslaw & Jaeger, 1959; Domenico & Schwartz, 1998):

$$\frac{\partial T}{\partial t} = D_t \left(\frac{\partial^2 T}{\partial x^2} + \frac{\partial^2 T}{\partial y^2} \right) - q \frac{\rho_w c_w}{\rho c} \frac{\partial T}{\partial x} \tag{1}$$

Equation 1 corresponds to the 2D advection-diffusion equation for a homogeneous and isotropic porous medium with a uniform and constant fluid flux q in x direction as proposed by Stallman (1965). In this equation, T is the temperature (K), q the groundwater flux (or specific discharge) (m/s), ρ_c the volumetric heat capacity of the rock–fluid matrix (J/m^3/K), and $\rho_w c_w$ the volumetric heat capacity of water (J/m^3/K). D_t is the thermal diffusivity coefficient (m^2/s) and depends on λ, the bulk thermal conductivity (W/m/K):

$$D_t = \frac{\lambda}{\rho c} \tag{2}$$

2.1.2. The Instantaneous Line Source Model

As highlighted by the heat transport equation, the temperature evolution is controlled by both the groundwater flux and the thermal properties of the saturated material, especially the thermal conductivity. Under

no-flow conditions ($q = 0$ in Equation 1), Carslaw and Jaeger (1959) showed that the differential equation for heat conduction could be solved for a homogeneous infinite medium, initially at thermal equilibrium (T_0 everywhere) by considering an Instantaneous Line Source (ILS). At $t = 0$, a constant linear heating power Q (W/m) is switched on. The temperature response ΔT ($\Delta T = T - T_0$) is given in x–y direction by

$$" T(x, y, t) = \frac{Q}{4\pi\lambda} \int_{\frac{r^2}{4tD_t}}^{\infty} \exp(-\Psi) \frac{\mathrm{d}\Psi}{\Psi} = \frac{Q}{4\pi\lambda}\left[-E_i\left(\frac{-r^2}{4tD_t} \right) \right] \tag{3}$$

where $r^2 = x^2 + y^2$ when the heat source is located at (0, 0), ΔT the change of temperature across the input time, and Ψ a change of variable:

$$\Psi = \frac{x^2 + y^2}{4D_t t} \tag{4}$$

The exponential integral function $-E_i(-1/x)$ is also known in hydrogeology as the Well-function $W(x)$. Thus, Equation 3 can be simplified by the Jacob approximation if t is sufficiently large or r very small, i.e., if $r^2/4D_t t << 1$ (Blackwell, 1954; de Marsily, 1976):

$$\Delta T = \frac{Q}{4\pi\lambda} W\left(\frac{4tD_t}{r^2} \right) \approx \frac{Q}{4\pi\lambda} \ln\left(\frac{2.25\,t\,D_t}{r^2} \right) \tag{5}$$

This assumption was used by Blackwell (1954) who developed a transient-flow method showing that the thermal conductivity λ could be extracted from the slope s of the linear regression between ΔT and $\ln(t)$ during the heating period:

$$s = \frac{\mathrm{d}T}{\mathrm{d}\ln(t)} = \frac{T(t_2) - T(t_1)}{\ln(t_2) - \ln(t_1)} = \frac{Q}{4\pi\lambda} \tag{6}$$

Recent applications of active-DTS methods in boreholes used this approach to estimate the distribution of thermal conductivities (Freifeld et al., 2008; Maldaner et al., 2019). However, the estimation of thermal conductivity in active-DTS applications achieved under flow conditions remains challenging due to the combined effects of both thermal conductivity and groundwater flux on the temperature increase.

2.1.3. The Moving Instantaneous Line Source Model

Carslaw and Jaeger (1959) proposed adapting the ILS model considering uniform flow across the heat source. They proposed solving the advection–conduction equation by considering a Moving Instantaneous Line Source (MILS) model that includes the effect of advection on the thermal response. By considering an initial thermal equilibrium T_0 and a constant and uniform heating rate power Q (W/m), the thermal response ΔT ($\Delta T = T - T_0$) along the line source can be expressed as

$$\Delta T(x, y) = \frac{Q}{4\pi\,\lambda} \exp\left[\frac{q\,x}{2D_t} \frac{\rho_w c_w}{\rho c} \right] \int_{\frac{x^2 + y^2}{4tD_t}}^{\infty} \exp\left[-\Psi - \left(\frac{x^2 + y^2}{D_t} \right) \frac{q^2}{16D_t\Psi} \frac{\rho_w^2 c_w^2}{\rho^2 c^2} \right] \frac{d\Psi}{\Psi} \tag{7a}$$

Different applications showed the potential of using this analytical solution to solve the advection–conduction equation for uniform and isotropic materials (Sutton et al., 2003; Zubair & Chaudhry, 1996). It is noteworthy that this solution can also be used for anisotropic material considering thermal dispersion (Carslaw & Jaeger, 1959; Metzger et al., 2004; Molina-Giraldo et al., 2011).

Having $r = \sqrt{x^2 + y^2}$, Equation 7a can also be written as

$$\Delta T = \frac{Q}{4\pi\,\lambda}\exp\left[\frac{q\,x}{2D_t}\frac{\rho_w c_w}{\rho c}\right]\int_{\frac{r^2}{4tD_t}}^{\infty}\exp\left[-\Psi-\frac{r^2\,q^2}{16D_t^{\,2}\,\Psi}\frac{\rho_w^{\,2}c_w^{\,2}}{\rho^2 c^2}\right]\frac{d\Psi}{\Psi}$$ (7b)

This equation can also be expressed using the Hantush Well-function $W(\alpha,\beta)$ (Hantush, 1956):

$$\Delta T = \frac{Q}{4\pi\,\lambda}\exp\left[\frac{q\,x}{2D_t}\frac{\rho_w c_w}{\rho c}\right]W(\alpha,\beta)$$ (7c)

where

$$\alpha = \frac{r^2}{4tD_t}$$ (8)

$$\beta = \frac{r\,q}{2D_t}\frac{\rho_w c_w}{\rho c}$$ (9)

$$W(\alpha,\beta) = \int_{\alpha}^{\infty}\frac{1}{\Psi}\exp\left(-\Psi-\frac{\beta^2}{4\Psi}\right)d\Psi$$ (10)

The MILS model (Equation 7a–7c) can be used to model and reproduce the temperature increase induced by a line heat source in an infinite medium. Considering this, Diao et al. (2004) described the behavior of the temperature increase under different flow conditions and demonstrated the impact of groundwater flow on performances of geothermal heat exchangers. They showed that the temperature increase is first mainly controlled by heat conduction for short times and then controlled by heat advection that dissipates the heat produced, which limits the temperature rise and leads to the stabilization of temperature for late time. For steady-state conditions ($t \to \infty$), they proposed to approximate Equation 7b using the Bessel function of second kind and order zero K_0:

$$\Delta T_f = \frac{Q}{2\pi\,\lambda}\exp\left[\frac{q\,x}{2D_t}\frac{\rho_w c_w}{\rho c}\right]K_0\left(\frac{rq}{2D_t}\frac{\rho_w c_w}{\rho c}\right)$$ (11)

where ΔT_f is the temperature reached for steady conditions. Diao et al. (2004) demonstrated that the duration t_s required to reach steady state, i.e., $\Delta T = 0.99\,\Delta T_f$, directly depends on the magnitude of the groundwater flux q:

$$t_s = \frac{4\lambda}{q^2}\frac{\rho c}{\rho_w^{\,2}c_w^{\,2}}$$ (12)

For short times, advection can be neglected, which means that the temperature increase can be modeled using the ILS model (Equation 5) considering only heat transfer by conduction. Since the behavior of temperature for steady-state conditions can be approximated by Equation 11, it is possible to define the intersection time t_i between the conduction-dominant stage, described by Equation 5, and the advection-dominant stage, described by Equation 11:

$$\frac{1}{2}\ln\left(\frac{2.25\,t_i D_t}{r^2}\right) = \exp\left[\frac{q\,x}{2D_t}\frac{\rho_w c_w}{\rho c}\right]K_0\left(\frac{rq}{2D_t}\frac{\rho_w c_w}{\rho c}\right)$$ (13)

By using the approximation $e^x K_0(x) \approx K_0(x) \approx -2.3\log_{10}(0.89x)$ (Hantush, 1956), the time t_i can be expressed as

$$t_i = \frac{2.24.\lambda}{q^2}\frac{\rho c}{\rho_w^2 c_w^2}$$ (14)

2.1.4. Applications for Active-DTS Experiments

The ILS and MILS models have been used to model temperature increase for different active-DTS applications. Bakker et al. (2015) and des Tombe et al. (2019) combined a vertical line heat source with a FO cable and used the MILS model to successfully reproduce the temperature increase measured all along the FO cable and to estimate groundwater fluxes. However, they did not consider the possible variations of thermal conductivity of the materials along the FO cable, which may increase the uncertainty on the estimated fluxes.

The application of the MILS model when using a single FO cable as a heat source and for temperature measurement has been seldom proposed. Among others, F. Selker and J. S. Selker (2018) offered to use the definition of the stabilization time (Equation 12), initially developed by Diao et al. (2004), to estimate the groundwater flux. Del Val (2020) recently studied the effect of the FO cable on the temperature increase. She showed that the evolution of the temperature measured in the cable is the combination of the heat propagation through the FO cable (ΔT_{FO}) with the heat propagation through the porous media (ΔT_{PM}):

$$\Delta T = \Delta T_{FO} + \Delta T_{PM} \tag{15}$$

For very small times ($t < 2$ min), the temperature evolution is driven by heat propagation through the FO cable, described by the authors as "the skin-effect." This effect is equivalent to the wellbore storage effect in groundwater hydraulics and depends on cable properties (diameter and thermal properties of the cable itself). It induces a relatively large increase of temperature ΔT_{FO} during the early period of heating due to the thermal properties of the FO cable. Considering the effect of the cable, she proposed a graphical interpretation of the flux based on the identification of the intersection time (Equation 14). However, the application of the method to a field case remains uncertain considering the error on flow estimation induced by noise in the data and the difficulty in removing the skin-effect and in defining t_i.

Besides these promising applications based on the use of the MILS model to interpret the temperature increase measured during active-DTS experiments, the method suffers from the lack of a standardized and validated interpretation method. In order to develop such a method, we present next a numerical model which considers all thermal processes controlling the temperature increase measured along a heated FO cable, namely heat transfer processes occurring through both the FO cable and the surrounding media. The aim is to highlight the effects of the FO cable, of the thermal properties of the media, and of the groundwater flow on the temperature rise in order to improve the understanding of the different thermal regimes controlling the thermal response over time. Numerical simulations will be used as a guide for developing and testing a theoretical interpretation methodology based on MILS models. This approach will be then validated using experimental data conducted during laboratory tests in a sandbox.

2.2. Numerical Model

As shown in Figure 1, the numerical model considers a simple 2D domain, within which heat transfer occurs with steady-state fluid flow in porous media. Simulations were done using the Conjugate Heat Transfer module of COMSOL Multiphysics®. Mesh size ranges from 4.85×10^{-6} to 2.68×10^{-2} m with the finest meshes around the FO cable. In order to simulate the thermal response for typical groundwater fluxes and to define the limitations of the method, the thermal response was modeled under a large range of flux ranging from 8×10^{-7} to 3×10^{-1} m/s. Defining the limitations of the method requires ensuring the stabilization of temperature expected under flow conditions, which involves long heating periods, especially for very low flow. After many tests, the heating period was set to 225 h, which necessarily involves the propagation of heat over a large domain whose dimensions depend on the groundwater fluxes. Thus, the size of the domain was adjusted for each flux tested to ensure that the heat produced does not reach the boundary of the domain (Thermal Insulation Boundaries). Under no-flow conditions, the domain was modeled as a square of 3×3 m with the heat source located in the center of the model. Under flow conditions, the domain is a rectangle whose size varies according to the flux: the increase of the flux requires increasing the length of the domain and reducing its width. For instance, the size of the model was set at 5×0.20 m for $q = 3 \times 10^{-5}$ m/s and the heat source was located 4 cm of the laminar inflow boundary condition. For $q = 3 \times 10^{-6}$ m/s, its size was set at 3×2.5 m with the heat source located at 0.90 m of the laminar inflow boundary condition.
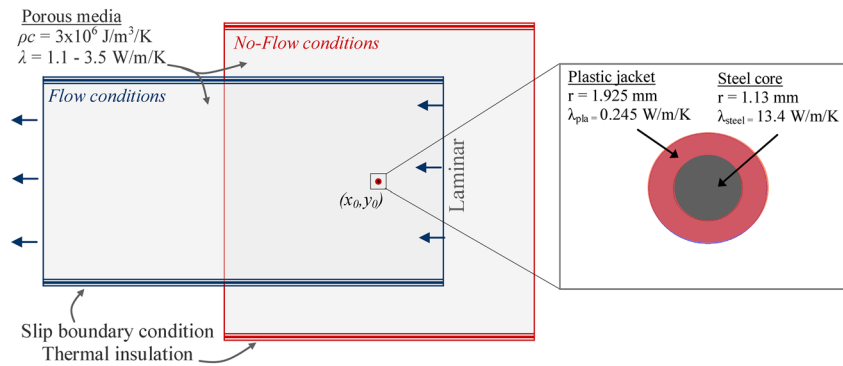
Figure 1. Numerical model geometry: the model simulates heat transfer by conduction with steady-state fluid flow using the Conjugate Heat Transfer module of COMSOL Multiphysics®. The thermal source (located at x_0 and y_0) was represented by a simplified FO cable considering the effect of the cable design on thermal storage and conduction. FO, fiber optic.

For each simulation, the size of the domain was validated by verifying the stability of the temperature near the boundaries for the whole heating period. A single and large domain, for instance, 5×5 m could have been used but it would have resulted in more significant run-time simulations, especially with the extra fine mesh size of the model. Considering the mesh size of the model as a characteristic length (COMSOL Multiphysics, 2019), the Courant number ranges between 2.88×10^{-4} and 0.62 and the Peclet number ranges from 5×10^{-3} to 0.91; such values lower than 1 ensure numerical stability.

The FO cable was explicitly implemented with a steel core and a plastic jacket to get a better understanding of the effect of the cable design (material, layer thickness, conductivity of materials) on the thermal response, following Read (2016). The plastic jacket and the steel core radius are defined in accordance with the cables used for field experiments, namely BRUSens cables (reference LLK-BSTE 85°C) whose external and steel tube diameters equal, respectively, to 3.8 and 2.2 mm. This simplified representation of the cable does not include all of its components, such as fiber optics or gel. Still, due to the high thermal conductivity of the steel, this representation is sufficient to reproduce heat transfer processes (Read, 2016), and thus the thermal response induced by the heated cable in the saturated porous medium. The active-DTS heat tracer experiment was simulated by applying a heat source term (W/m^3) in the steel core, defined as the ratio between the electrical power input (W/m) and the surface of the steel core (m^2).

Temperature variations throughout the domain and in the cable core were first modeled under no-flow condition, for $q = 0$ m/s, with heat transfer being exclusively controlled by conduction. Then, simulations were conducted by sweeping the groundwater flux over a range of 10^{-17} to 3×10^{-1} m/s. All simulations were performed using two values of thermal conductivity for the porous media, i.e., $\lambda = 1.1$ and 3.5 W/m/K, which allows covering a large range of thermal conductivities commonly found for sedimentary aquifers (Stauffer et al., 2013). Durations of heating periods were adjusted according to flow to ensure temperature stabilization at late times. Temperature distributions during recovery, after the end of heat injection, were also simulated to obtain the evolution of temperature during both heating and recovery periods.

2.3. Sandbox Laboratory Experiments

2.3.1. Experimental Setup

Laboratory experiments were conducted in a sandbox in which flow rates can be well controlled in order to test the proposed active-DTS interpretation method on experimental data. As shown in Figure 2, active-DTS experiments have been conducted by deploying a FO cable in a 0.576 m^3 PolyVinyl Chloride tank open at the top (1.6 m long, 1.2 m width, and 0.3 m height) and filled with 0.4–1.3-mm-diameter quartz sand that comprises 12% of fine sand, 28% of medium sand, and 60% of coarse sand. The height of water in reservoirs on two sides of the sandbox (h_1 and h_2) can be adjusted manually to control of hydraulic gradient and thus the water flow through the sand. The setup of the sandbox is such that flow can be considered homogeneous. The average hydraulic conductivity was estimated at 3.06×10^{-3} m/s (Table 1). This experiment was
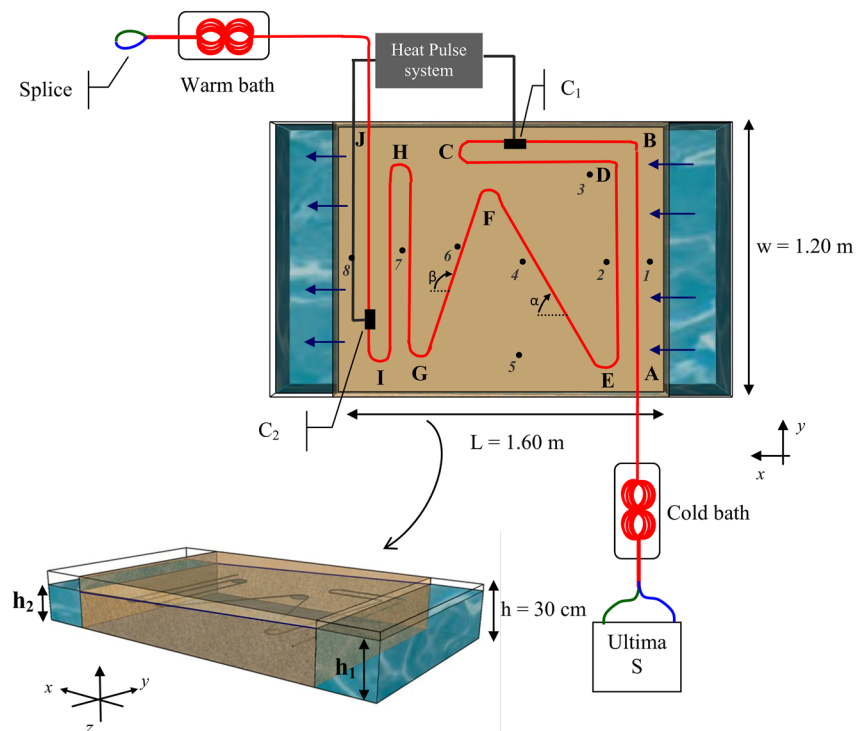
Figure 2. Experimental setup showing the dimensions of the sandbox and the deployment of FO cable (top view [x,y plane] and side view [x,y,z plane]). The marks C_1 and C_2 represent the electric connections between the FO cable and the electrical cables allowing the injection of electricity into the steel frame of the FO cable (modified from Simon et al., 2020). FO, fiber optic.

the subject of a precedent study whose aim was to discuss the feasibility of conducting active-DTS measurements in a sandbox knowing that the spatial resolution of DTS units could be close to the size of the experiment. More details about the experimental setup are provided in Simon et al. (2020).

The cable was buried inside the sandbox at 20 cm-depth below the sand surface. The cable was installed so that the angle between the flow and the FO cable varies in space. Cable sections called DE, HG, and HI are perpendicular to water flow (90°), whereas cable section CD is parallel to water flow. Sections EF and FG lie, respectively, at a 60° angle (α) and a 110° angle (β) to the water flow direction. The FO cable used is a 3.8-mm-diameter cable containing four multimode 50/125-μm fibers (BruSens cable; reference LLK-BSTE 85°C). As shown in Figure 2, two fibers were spliced at the end of the cable, allowing measurements in double-ended configuration (van de Giesen et al., 2012). The paired fiber was connected to a Silixa Ultima S DTS unit reporting temperature every 12.5 cm at a-20 s sampling interval (10 s per channel). The effective spatial resolution of the unit was experimentally estimated during heating periods to be between 51 and 67 cm (Simon et al., 2020). To calibrate the DTS unit, 20 m of cable was placed in a warm calibration bath and 20 m in a cold calibration bath (a box filled with wetted ice). In each bath, a PT100 probe (0.1°C) and a RBR SoloT probe (0.002°C accuracy) recorded the temperature to calibrate the acquired data. With this setup, the relative uncertainty of measurement was estimated to 0.03°C while absolute uncertainty of measurement can be estimated at 0.15°C. External temperature probes, marked from 1 to 8 in Figure 2, allowed monitoring temperature variations in the sandbox at different distances from the FO cable.

2.3.2. Heat Tracer Experiments

A 7-m section of cable was electrically isolated and connected to an electrical cable (connections C_1 and C_2) to allow the injection of electricity from a power controller. A succession of active-DTS experiments was conducted under different flow rates for 4 days to characterize the effect of flow on the thermal response. As shown in Table 1, the recovery period following each heating was monitored at least 14 h after turning off the power controller, ensuring the return to the ambient temperature. The flow rate through the sandbox

Table 1
Details of Experimental Conditions During the Experiment

		Day 1	Day 2	Day 3	Day 4
Experimental conditions	Flow rate (m³/s)	2.12×10^{-5}	1.33×10^{-5}	4.8×10^{-6}	0
	Duration of heating period	04h20m	08h00m	08h05m	08h00m
	Injected power (W/m)		20		
	Duration of recovery period (h)	15	15	14	20
Calculated parameters	Hydraulic conductivity (m/s)	$3.12 \times 10^{-3} \pm 1.29 \times 10^{-4}$	$3.24 \times 10^{-3} \pm 2.54 \times 10^{-4}$	$3.06 \times 10^{-3} \pm 7.98 \times 10^{-4}$	
	Flux (Darcy velocity) (m/s) along section DE	4.93×10^{-5}	2.95×10^{-5}	1.11×10^{-5}	0

was progressively decreased, until the no-flow condition was reached ($q = 0$). For each experiment, the flow rate was measured independently and manually at the outlet of the bench. The hydraulic conductivity was calculated using Darcy's law under unconfined conditions. An estimate of the water flux according to the distance from the inlet reservoir (h_1) was also calculated (Domenico & Schwartz, 1998). Table 1 provides details about flow conditions for each day of the experiment and the estimate of the hydraulic conductivity and water flux for section DE (located 20 cm from the inlet reservoir). For each experiment, the cable was energized continuously during a few hours (between 6 and 8 h) using a Silixa Heat Pulse Control System, delivering a well-controlled power intensity of 20 W/m along the heated section, by injecting continuously 141 W in the electrical circuit with an input amperage of 7.4 A.

Considering the spatial resolution of the DTS device and the limited size of the sandbox, the feasibility of conducting active-DTS experiments in such conditions was discussed in a previous publication (Simon et al., 2020). We validated experimental results for most measurement points, except section GH that was highly affected by heated adjacent sections of cable. In addition, we have ensured and verified that the boundaries of the tank were not affected by the heat injection along the FO cable.

3. Results

3.1. Numerical Simulations Results

Figure 3a shows the evolution of the simulated temperature during heating under different flow conditions. The log-time derivative of temperature is shown along the temperature evolution to highlight the effect of the different processes following Renard et al. (2008). During the first seconds of heat injection through the steel armoring of the cable, the evolution of both the temperature and its derivative is similar independently of the water flux. The temperature increases very rapidly and ΔT reaches 16.8°C in about 100 s. After few seconds, the derivative departs from the temperature curve and makes a hump. Afterward, the thermal response depends on flow conditions. When heat transfer is exclusively by conduction ($q = 0$ m/s), a gradual and continuous increase of temperature is observed over time and the log-time derivative tends toward a constant value of 2.51 (solid and dotted red lines).

Under flow conditions (green, orange, and blue lines), the temperature stabilizes progressively at late time. The associated log-time derivative decreases continuously before stabilizing toward zero. The value of ΔT after temperature stabilization depends on groundwater flux. As expected, the higher the water flux, the lower the value of ΔT. For each example, characteristic times t_d and t_a are defined and highlighted, since these times allow a proper characterization of q as we will see in the following sections. Time t_d corresponds to the moment when the temperature curves under flow conditions separate from the curve under no-flow conditions and when the associated log-time derivatives start decreasing. Time t_a corresponds to the moment when temperature stabilizes and the log-time derivative reaches zero. As shown in Figure 3a, these two characteristic times depend also on the magnitude of flux.

The analysis of the behavior of both the temperature and its log-derivative in the semilogarithmic plot appears efficient to delimitate the effect of the different parameters on the temperature increase. Thus, by analogy with well-test interpretation, the hump made by the log-derivative in early times can be interpreted
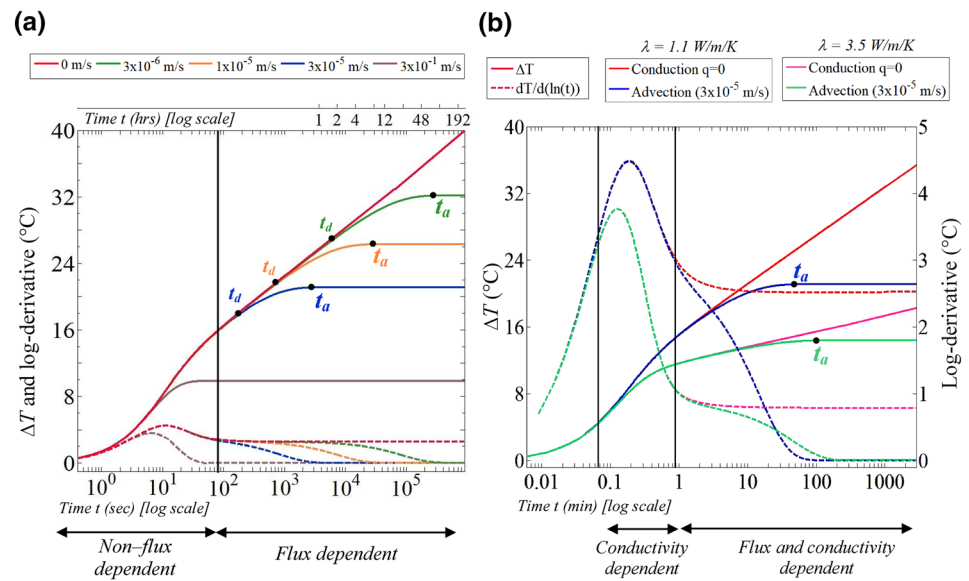
Figure 3. Typical examples of thermal responses obtained from active-heating experiments simulated using the numerical model described in Section 2.2. These curves highlight (a) the effect of groundwater flux on both the temperature (solid curves) evolution and its derivative (dotted curves) and (b) the effect of thermal conductivity and flow conditions on both the temperature evolution (solid curves) and its derivative (dotted curves).

as the result of "storage effects" (Del Val, 2020; Papadopulos & Cooper, 1967; Renard et al., 2008), which clearly helps to delimitate the period when temperature increase is affected by the FO cable. Moreover, temperature stabilization, which should be reached once the heat injected through time is fully dissipated by heat advection, could be investigated through the log-derivative similarly to case of leaky aquifers or constant head boundary aquifers that are identified through the behavior of drawdown evolution (Hantush, 1956; Hantush & Jacob, 1955; Renard et al., 2008).

Figure 3b shows the evolution of both temperature and log-time derivative of simulated temperature during heating periods under different flow conditions and for different porous medium thermal conductivities. During the first 20 s of heat injection, the responses are fully independent of both flux and thermal conductivity. Afterward, temperature increases independently of flow for a few minutes. During this period, the temperature increase is higher for a smaller thermal conductivity. At later times, the thermal response depends on both thermal conductivity and flow that dissipates the heat produced, leading to temperature stabilization. The higher the thermal conductivity, the lower the value of ΔT.

3.2. Description of the Typical Thermal Response Curve

Numerical simulations highlight the role of the distinct heat transfer processes on the temperature rise during active-DTS experiments. These numerical results will provide the basis for the proposed general interpretation of thermal response curves and allow the definition of the typical response curve expected under flow conditions during active-DTS experiments using the FO cable as the heat source. Figure 4a illustrates this typical response and indicates the heat transfer processes at play in different stages of the temperature rise during heating.

As shown in Figure 4a, the temperature increase during the experiment is the result of the combination of the effect of the FO cable (ΔT_{FO}) and the heat transfer occurring through the porous media (ΔT_{PM}). ΔT_{FO} is the result of the heat storage and heat conduction occurring through the FO cable from the beginning of the heat injection. The hump made by the curve of the log-time derivative shows that these processes affect the temperature increase only during a short period, from the start of heating to time t_c. As soon as the heat produced reaches the surrounding material, thermal heat processes occurring through the porous media begin to control the temperature increase. After a very short time, the temperature increase depends on the
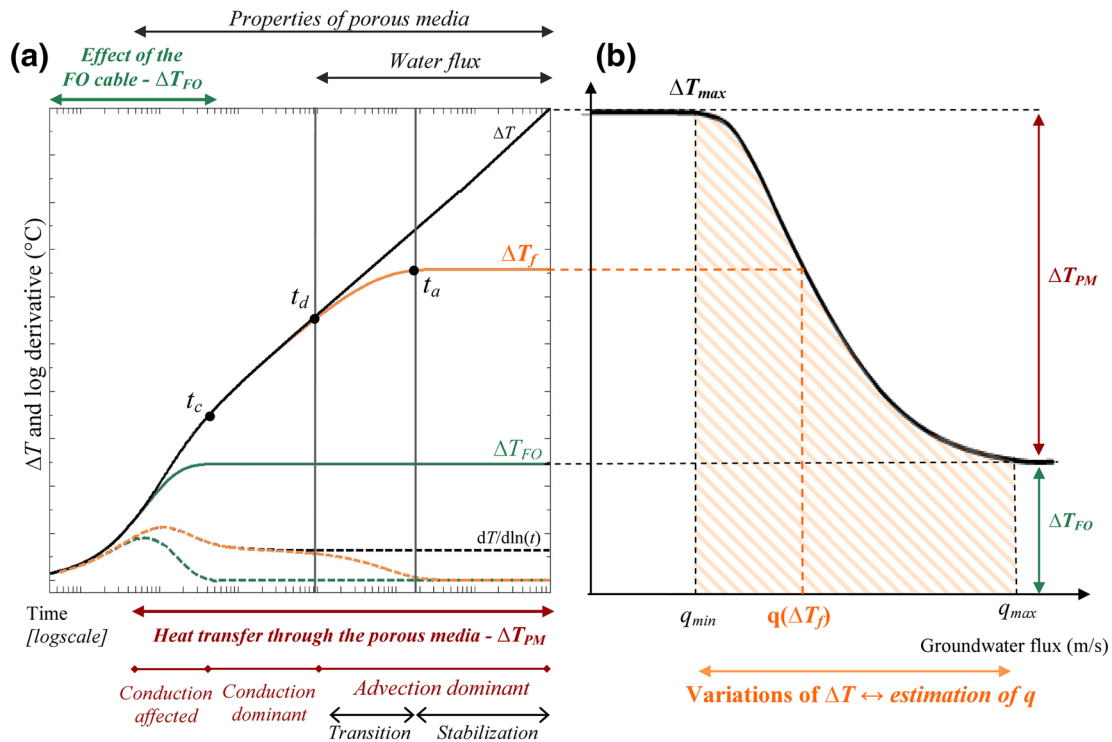
Figure 4. (a) Theoretical thermal response curves showing the effect of heat transfer processes on the temperature increase measured during heating. The orange curve describes the typical response curve expected during an experiment. The black and brown curves correspond to the behavior expected for extreme and specific hydraulic conditions, respectively when $q \rightarrow 0$ and for high groundwater flux. (b) Schematic evolution of the value of $\Delta T_f(t)$ depending on groundwater flux after a given heating time t.

thermal properties of the porous media (as demonstrated in Figure 3b). For a short period, the evolution of the temperature is thus simultaneously controlled by heat conduction and storage in the cable as well as heat transfer occurring in the porous medium (conduction-affected stage).

For $t > t_c$, temperature variations are no longer sensitive to the effect of the heated FO cable and the temperature rise is exclusively controlled by heat conduction through porous medium in accordance with Equation 5. This gradual increase of temperature observed from $t = t_c$ up to $t = t_d$ corresponds to the "conduction-dominant period." When t exceeds t_d, the temperature rise departs from the conduction regime with a decreasing rate of temperature rise. Time t_d can be defined as the limit between the conduction-dominant stage and the advection-dominant stage, which should occur for a thermal Peclet number $Pe = 1$. A transition period is then observed between t_d and t_a, after which time the temperature stabilizes at the maximum temperature $\Delta T(t) = \Delta T_f$. After $t = t_a$, advection is clearly dominant and the heat injected is fully dissipated by advection and conduction in the porous medium.

Further insights on the thermal response is provided in Figure 4b, which shows the temperature variation reached after a specific heating time t, $\Delta T(t)$, depending on groundwater flux. Figure 4b clearly shows that for a given thermal conductivity, a broad range of fluxes, between q_{min} and q_{max}, can be estimated from the temperature rise ΔT_f. For $q < q_{min}$, advection is negligible and conduction dominates heat transfer, the temperature response being insensitive to flow. For $q > q_{max}$, the temperature rise is limited to the temperature increase induced by the FO cable, ΔT_{FO}, most of the heat produced being dissipated by advection except the one stored within the FO cable. It should be noted that the typical response curve (orange curve in Figure 4a) can be observed between q_{min} and q_c (orange hatched area). Between q_c and q_{max}, the conduction-dominant period is negligible, meaning that ΔT_{PM} is entirely controlled by advective heat transfers occurring through the porous media. Despite that, between q_{min} and q_{max}, each value of q can thus be associated with a single value of ΔT_f. The uncertainty associated with groundwater flux estimates can be also easily deduced from Figure 4b, knowing the accuracy of temperature measurements.
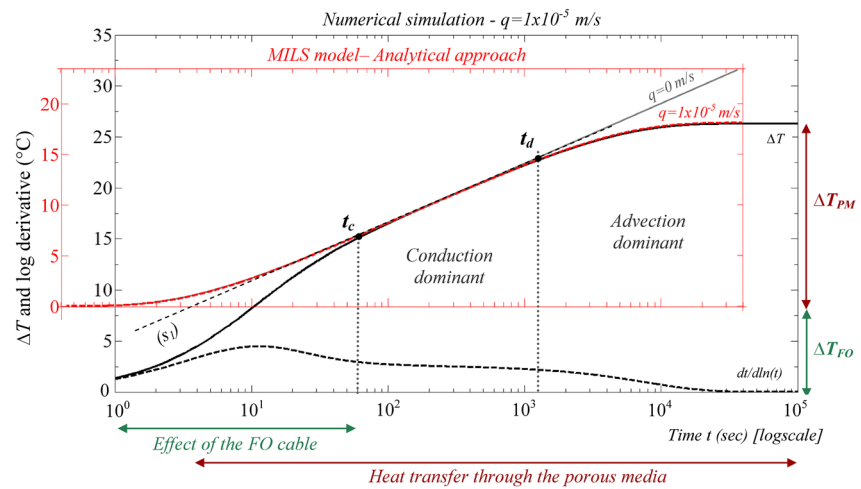
Figure 5. Application of the MILS model to reproduce the temperature increase observed during the second stage of the thermal response curve. In this example, the approach was tested using one of the thermal response curves numerically simulated (black line) considering $\lambda = 1.1$ W/m/K and $q = 1 \times 10^{-5}$ m/s (see Section 2.2). The analytical solution can be used to reproduce the temperature evolution (i) during the conduction-dominant period only by considering $q = 0$ m/s and $\lambda = 1.1$ W/m/K (gray line) and then (ii) during the advection-dominant period (red dotted line) by considering the effective value of the flow ($q = 1 \times 10^{-5}$ m/s) once the thermal conductivity is defined. Then, the extrapolation of the MILS model for $t < t_c$ provides an estimate of ΔT_{FO}, and therefore of ΔT_{PM}. MILS, Moving Instantaneous Line Source.

3.3. Interpretation of the Thermal Response Curve

3.3.1. The Use of the MILS Model

The behavior of the temperature evolution through time described in the previous section has important consequences for the interpretation of temperature data obtained from active-DTS experiments. The analytical solution from Des Tombes et al. (2019) cannot be used directly here since the increase in temperature associated with heat conduction within the FO cable is not considered. As shown in Figure 3, this difficulty is due to the fact that the temperature increase during the first stage of the thermal response is simultaneously controlled by heat transfers occurring through the FO cable and by heat conduction occurring through the porous medium. In the following, we propose an interpretation method that accounts for the effect of the FO cable and provides independent estimates of the varying thermal properties of the porous media and the groundwater flux.

As shown in Figure 5, the interpretation focuses on the second part of the thermal response curve, when the temperature increase is only controlled by heat transfer occurring through the surrounding porous media and thus driven by heat conduction and advection, using the MILS model. First, the approach requires the identification of time t_c corresponding to the duration of the first stage of the thermal response, during which heat conduction occurs mainly through the FO cable. This really short delay (around 50 s here) is marked by the end of the hump made by the log-time derivative of temperature and can be graphically defined both by the shape of the log-derivative of temperature and by the fact that the conduction-dominant period should be apparent as the start of the straight line increase in temperature from $t = t_c$ (straight line s_1 in Figure 5).

Once t_c is defined, the MILS model (Equation 7a–7c) can first be used by considering $q = 0$ m/s (gray line) to reproduce the temperature increase occurring during the conduction-dominant period (i.e., for $t_c < t < \sim1,000$ s in Figure 5). Here, the temperature increase during the conduction-dominant period can be perfectly reproduced by the analytical solution Root-Mean-Square Error (RMSE) < 0.01°C) by applying a value of λ equal to 1.1 W/m/K, in perfect agreement with the thermal conductivity considered in the numerical model. Thus, this approach can provide a direct estimation of the thermal conductivity of the porous media. Knowing the value of thermal conductivity, the temperature increase can be then modeled for any $t > t_c$ using the MILS model considering both the previous value of thermal conductiv-
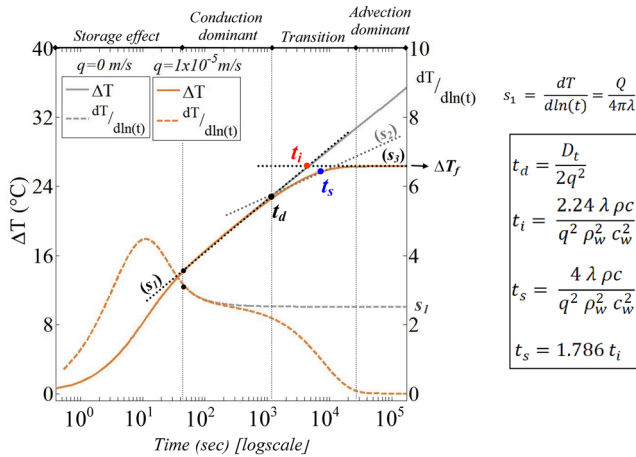
Figure 6. Graphical interpretation of the thermal response: definition of the characteristic times t_d, t_i, and t_s to estimate groundwater flux and calculation of slope s_1 during the conduction-dominant period to evaluate thermal conductivity.

ity and the unknown value of groundwater flux. Here, by considering $q = 1 \times 10^{-5}$ m/s (dotted red line in Figure 5), the MILS model reproduces perfectly the temperature evolution during both the conduction-dominant and the advection-dominant periods (RMSE $\approx 0.02°C$). Thus, this simple approach can provide a direct and precise estimation of both the thermal conductivity of the porous media and the flux. By deduction, this approach also provides a direct estimation of the effect of the cable ΔT_{FO} on the thermal response whose direct quantification remains otherwise difficult.

3.3.2. Graphical Interpretation of the Thermal Response Curve

In this section, we propose another complementary approach to interpret the temperature evolution through time by defining characteristic times related to groundwater flux. As shown in Figure 6, under flow conditions (orange line), the different heat transfer regimes can be easily defined and delimited by well-marked changes in temperature evolution. The change in temperature is linear in the semilogarithmic plot under both the conduction-dominant period and the stabilization-time period, which are respectively characterized by straight lines with slopes s_1 and s_3. The temperature trend during the transition-time period can also be approximated by a slope s_2. Again, it is important to clearly define the transition period to avoid any misinterpretation with the conduction-dominant period and to ensure a correct determination of the characteristic times.

As shown in Figure 6, the transient-flow method for determining the thermal conductivity developed by Blackwell (1954) (Equation 6) can be applied to determine slope s_1 under the conduction-dominant period. The duration of the conduction-dominant period is variable and depends on both thermal conductivity and groundwater flow. The slope should be estimated from the end of the hump of the log-derivative to the start of temperature stabilization, marked by the slope change to s_2. The numerical simulations presented in Figure 3 were used to graphically estimate the thermal conductivity using the calculated slope s_1. The thermal conductivity was exactly estimated for each simulation, with a mean standard deviation of 0.07 W/m/K. Under no-flow conditions, the derivative tends toward the value of the slope s_1 (2.51 on the example in Figure 6). Under flow conditions, the estimation is less accurate for high fluxes (± 0.2 W/m/K when $q = 3 \times 10^{-5}$ m/s and ± 0.03 W/m/K when $q = 3 \times 10^{-6}$ m/s) because the conduction-dominant period is shorter and therefore more difficult to delimitate. Note also that the use of this approach requires that Equation 3 can be approximated by the Well-function, i.e., that $r^2/4D_t t \ll 1$ (Blackwell, 1954; de Marsily, 1976). Here, considering the very small diameter of the FO cable (r), this condition is satisfied as soon as t is greater than a few seconds (for $\lambda = 2$ W/m/K and $\rho_c = 3 \times 10^6$ J/m^3/K).

In addition, it is possible to use the intersection time t_i defined as the intersection between the conduction-dominant period and the advection-dominant period to estimate groundwater flux (Equation 14). This time can be easily estimated graphically when both slopes s_1 and s_3 are well defined and when the transition period is clearly identified. Similarly, the flux may be estimated from characteristic time t_d, which corresponds to the intersection point between slopes s_1 and s_2. For $t = t_d$, the thermal Peclet number should equal 1 so that

$$Pe = \frac{dq}{D_t} = 1 \tag{16}$$

with d the characteristic length that can be represented by the mean grain size (Stauffer et al., 2013). By assuming that the characteristic length at $t = t_d$ corresponds to the diffusion length, d can be defined as $d = \sqrt{2D_t t_d}$ leading to

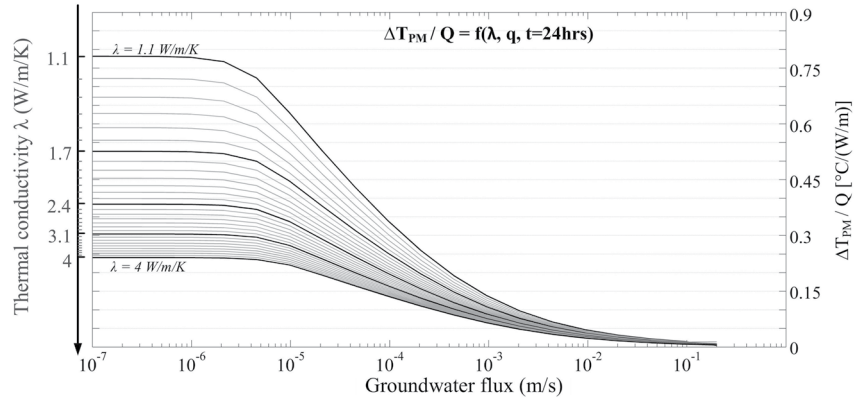$$q = \sqrt{\frac{D_t}{2 t_d}} \tag{17}$$

Figure 7. Theoretical curves $\Delta T_{PM} = f(q, t = 24\,h)$ showing the expected value of ΔT_{PM} depending on groundwater flux and thermal conductivity.

Lastly, the groundwater flux can also be defined through the steady-state time t_s reached when $\Delta T = 0.99\,\Delta T_f$ (Equation 12) (Diao et al., 2004; F. Selker & J. S. Selker, 2018).

To summarize, the groundwater flux can be estimated graphically by defining the three characteristic times t_d, t_i, and ts:

$$q \approx \sqrt{\frac{\lambda}{2\,\rho c\,t_d}} \approx \sqrt{\frac{2.24.\lambda}{t_i}\frac{\rho c}{\rho_w^{\,2} c_w^{\,2}}} \approx \sqrt{\frac{4\,\lambda}{t_s}\frac{\rho c}{\rho_w^{\,2} c_w^{\,2}}} \tag{18}$$

The equivalence below may be verified to validate the estimation of characteristic times:

$$t_s = 1.786\,t_i \tag{19}$$

One of the main advantages of this method is that these times are completely independent of the effect of the FO cable on temperature rise. Values of groundwater flux were estimated for each numerical simulation using the graphical approach by determining the characteristic times t_d, t_i, and t_s. The application of the graphical method provides a very good estimate of the flux with a mean error of around 4.7%. The error on the estimation increases with the increase of flux magnitude and reaches 7.4% when $q = 3 \times 10^{-5}$ m/s against 1.3% when $q = 3 \times 10^{-6}$ m/s.

3.3.3. Expected Increase of Temperature

The analytical solution can also be used to define theoretical curves $\Delta T_{PM} = f(q, \lambda, t)$ that can relate each value of ΔT_{PM} with a value of flux q, estimated for a specific heating duration t, and a given thermal conductivity λ, as illustrated in Figure 7. For a given heating duration once λ is estimated, such curves can provide a direct estimation of the flux if the temperature increase due to the FO cable (ΔT_{FO}) has been previously estimated. These curves can also help to define more precisely the limits of the method and especially the values of q_{min} and q_{max}, beyond which the flux estimate is not possible. Note that, in accordance with Equations 7, the temperature increase is proportional to the injected power Q. Thus, these theoretical curves can be established for either a specific value of power, $\Delta T = f(q, \lambda, t, Q)$, or normalized, $\Delta T/Q = f(q, \lambda, t)$. In practice, the normalization of the temperature increase by the injected power can help to compare results conducted under different conditions and verify the reproducibility of measurements.

3.4. Experimental Validation

3.4.1. Experiments Results

Figure 8a shows the evolution of the mean temperature measured along section DE during the experiment, which constitutes the ideal case in which the cable is perpendicular to flowing water (Figure 2). Considering the flow direction and the transport of heat generated along the cable from upstream to downstream (from
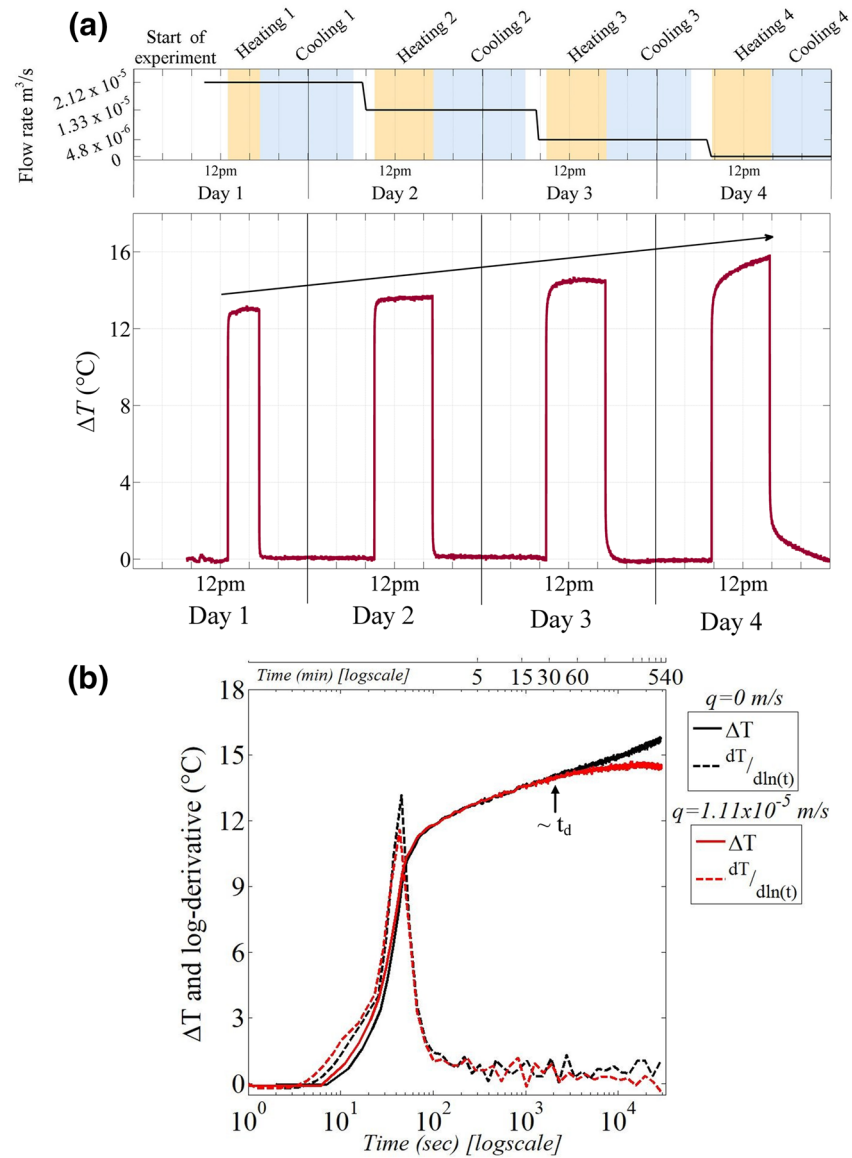
Figure 8. (a) Succession of active-DTS experiments conducted under different flow conditions and evolution of the mean temperature increase, ΔT, recorded along section DE during heating and recovery periods. (b) Evolution of the temperature increase (solid lines) and the log-time derivative of temperature (dotted lines) for a flow rate of 4.8×10^{-6} m³/s (red lines; Day 3) and under no-flow conditions (black lines; Day 4).

DE to IJ), section DE is the only one whose temperature evolution is not affected by upstream heated sections. The representativeness of DTS measurements along this section was validated by Simon et al. (2020) who studied the effective spatial resolution during active-DTS experiment using the same data set as the one used in this study. The value ΔT corresponds to the difference between the temperature measured over time and the initial temperature. For each experiment, the start of the heating period (yellow periods in the top of Figure 8a) and the start of the recovery period (blue periods in the top of Figure 8a) induce rapid and sharp temperature changes (at least 12.5°C in less than 3 min). As expected, the lower the flow rate or flux, the higher the ΔT reached at the end of the experiment. Note also that the inflow temperature changed slightly over time, mainly due to the loop water circulation, affecting the thermal response. Thus, data were postprocessed by applying a filter based on the propagation and the attenuation of temperature changes inside the sandbox using classical heat transport equations (Anderson, 2005; Domenico & Schwartz, 1998) in order to keep only the temperature variations induced by the heat injection (Simon et al., 2020).
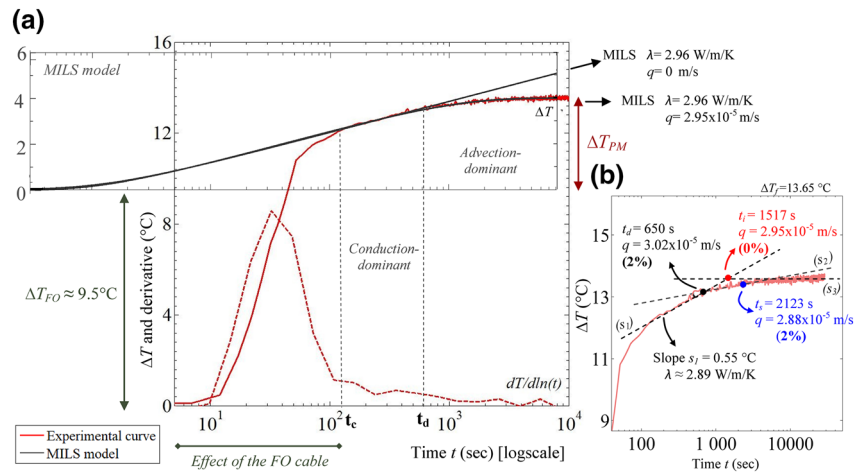
Figure 9. (a) Interpretation of the thermal response curve (red solid line) obtained during the second day of the experiment ($q = 2.95 \times 10^{-5}$ m/s). The dotted red line represents the log-time derivative of temperature. The temperature rise was matched with the MILS model (black lines) (Equation 7a) for $q = 0$ m/s (for $t_c < t < 600$ s) and $q = 2.95 \times 10^{-5}$ m/s (for $t > t_c$). In the MILS model (Equation 7a), the distance (x,y) between the heat source and the measurement point was fixed to $x = 1.9 \times 10^{-3}$ m and $y = 0$ m, considering flow in the y direction, with x the effective radius of the FO cable used during the experiment and measured using an electronic caliper. (b) Application of the proposed graphical method based on the recognition of three characteristic times allowing the estimation of groundwater flux. The percentage of error of q estimates obtained from the three characteristic times compared to the experimental measurement of q is indicated. The graph highlights the last part of the temperature curve to better show characteristic times. MILS, Moving Instantaneous Line Source; FO, fiber optic.

Figure 8b shows the evolution of temperature and its log-time derivative measured under no-flow (black lines) and flow conditions (4.8×10^{-6} m³/s, red lines). During the first 30 min of heat injection, the temperature evolution is similar for both curves independently of flow conditions. The temperature increases very rapidly in the first 2 min with ΔT reaching 12°C. Then, the temperature keeps increasing gradually with ΔT reaching 13.9°C after 30 min of heat injection. Afterward, the temperature evolution under flow conditions (red lines) departs from the temperature evolution under no-flow conditions and stabilizes progressively around 14.5°C, meaning that steady state is reached. Concerning the evolution of the log-derivative of temperature (dotted lines), the derivative makes a hump at very short times and seems to stabilize for times greater than 2 or 3 min.

Thus, the temperature evolution with time measured along the section DE seems in very good agreement with the expected behavior. Results show (i) a gradual and continuous increase of temperature under no-flow conditions (Carslaw & Jaeger, 1959); (ii) the effect of advection on the late thermal response under flow conditions (Carslaw & Jaeger, 1959; Diao et al., 2004; Zubair & Chaudhry, 1996); (iii) that higher values of ΔT can be associated with lower flow velocities (Bakx et al., 2019; Perzlmaier et al., 2004), and (iv) the effect of heat storage within the cable is limited to the early moments of heating, as highlighted by the characteristic behavior of the derivative (Del Val, 2020). To go further, these promising data will be used in the following sections to apply and validate the two interpretation methods previously described, i.e., the MILS model and the graphical approach.

3.4.2. Detailed Application of the Interpretation Methods

Figure 9 provides an example of the interpretation of the thermal response curve obtained during the second day of the laboratory experiment ($q = 2.95 \times 10^{-5}$ m/s). Figure 9a focuses on the use of the MILS to reproduce the temperature evolution during the second stage of the curve ($t > t_c$). The first step of the interpretation workflow consisted in defining the time t_c, from which the temperature increase is exclusively controlled by heat transfer through the porous medium. In this example, t_c is around 110 s, which corresponds to the end of the hump made by the log-time derivative of temperature and the start of the conduction-dominant period.

In the next step of the interpretation workflow, the MILS model considering $q = 0$ m/s (Equation 7a representing a line in the semilog graph) was used to estimate the effective value of thermal conductivity for $t_c < t < 600$ s. For that purpose, the MILS model was used with a range of values of thermal conductivity (from 1 to 4.5 W/m/K with a step of 0.01 W/m/K). For each value of thermal conductivity, the RMSE between the predicted model and the measured temperature during the conduction-dominant period was calculated. The optimal value of the estimated thermal conductivity with the lowest RMSE (0.04°C) was found at $\lambda = 2.96$ W/m/K (black line in Figure 9a).

For the following step of the interpretation workflow, the flux q can be estimated by varying q in the MILS model (Equation 7a) with the previously estimated value of thermal conductivity. The optimal value of q is the one leading to the lowest RMSE between the MILS and the observed temperatures from the start of the conduction-dominant period ($t > t_c$) until the end of heating. For the experimental results, the previously estimated thermal conductivity ($\lambda = 2.96$ W/m/K) was used in the MILS model together with the value of q (2.95×10^{-5} m/s) estimated experimentally. With this value of q, the MILS model perfectly reproduced the experimental data with a RMSE between the experimental data and the MILS model around 0.1°C (Figure 9a).

The application of the MILS model with the optimal values of thermal conductivity λ and flux q also allows the estimation of the two parts of the active-DTS temperature rise respectively related to the porous media ΔT_{PM} and to the FO cable ΔT_{FO} (Figure 9a). Although it occurs over a very short period, the effect of the FO cable properties can thus be experimentally observed through the behavior of the log-time derivative of temperature (dotted red line in Figure 9a). The data interpretation can be also based on the evolution of the log-time derivative of temperature for later times ($t > t_c$) which is however more difficult to achieve since the calculated derivative is noisy. The noise in the derivative is greatly dependent on the temperature resolution and sampling time of the DTS device. This point is a classical issue when calculating the derivative of experimental data, especially for well-test interpretation (Ramos et al., 2017; Renard et al., 2008).

As shown in Figure 9b, the graphical approach was similarly applied to estimate both the thermal conductivity and the flux. The temperature evolution at intermediate and late times was approximated by the three different slopes s_1, s_2, and s_3. The value of the slope of each interval that can be defined within the conduction-dominant period by varying the duration (5 points minimum) and the bounds of the considered interval was calculated. The average and standard deviation of slope estimates with $R^2 > 0.98$ was calculated, providing a rough estimate of the thermal conductivity of the saturated porous media (Equation 6), equal to 2.89 ± 0.32 W/m/K, in very close agreement with the previous estimate. Then, characteristic times t_d, t_i, and t_s (Figure 9b) were defined to provide independent estimates of flux (Equation 18), which are also in very good agreement with the expected value from the laboratory measurement. Note that values of the volumetric heat capacity of water ($\rho_w c_w$) and of the porous medium (ρ_c) were fixed at 4.1×10^6 and 3×10^6 J/m³/K, respectively. The effect of the volumetric heat capacity of the porous medium will be discussed next.

3.4.3. Interpretation of the Different Experimental Thermal Curves

As shown in Figure 10, the two proposed interpretation methods were also applied to the temperature evolution measured for each day of the experiment described in Section 3.4.1.

Figure 10a shows that the thermal conductivity was graphically estimated for each experiment (gray lines) by calculating the slope during the conduction-dominant period. Under no-flow conditions (dark blue line), the thermal conductivity is evaluated at 2.89 ± 0.2 W/m/K. This result is consistent with the common range of thermal conductivity of saturated sands, varying from 1.5 to 4 W/m/K (Stauffer et al., 2013) and can be considered here as the actual thermal conductivity of the saturated sand. Under flow conditions (green, red, and light blue lines), the duration of the conduction-dominant period is shorter for higher fluxes. The estimated values of thermal conductivity are still very close from the reference value. Of course, the uncertainty is higher for higher fluxes ($\sigma = 0.45$ W/m/K for the highest flux) because of the shorter duration of the conduction-dominant period. The graphical estimation of flux based on the determination of characteristic times also provides very good results for the different experiments, with a maximum error of 6%. Results for the first and the third experiments are not shown since they are very similar to the examples described in the previous section.
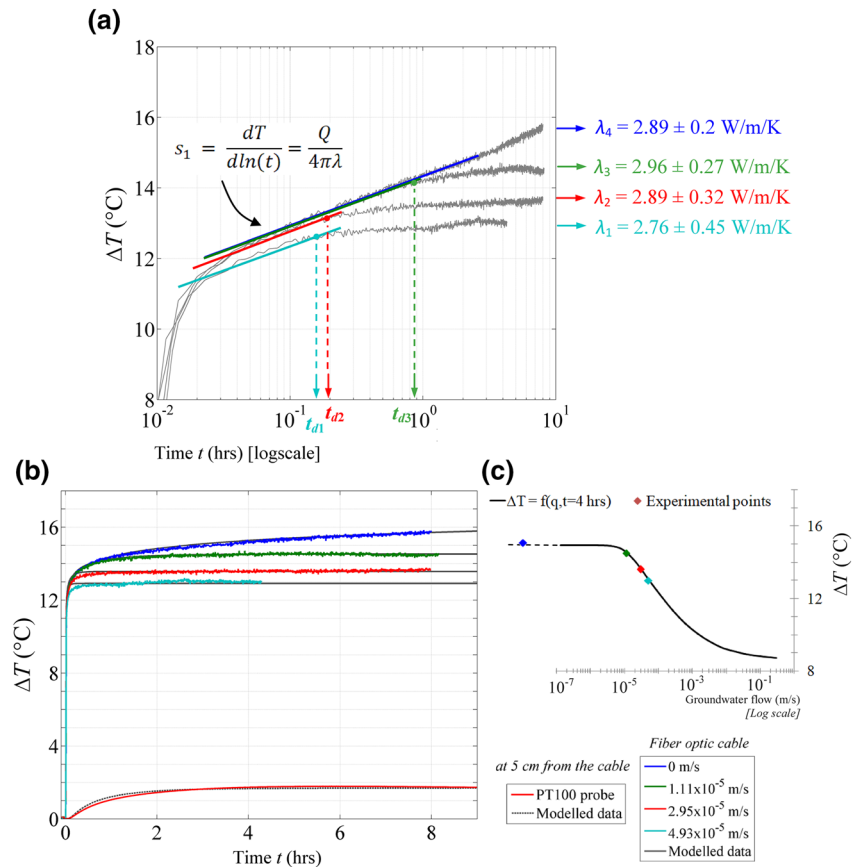
Figure 10. (a) Estimation of thermal conductivity under the different flow conditions using the slope s_1 during the conduction-dominant period. For each flux, the slope used to estimate thermal conductivity λ is shown. (b) Use of the MILS model to reproduce thermal responses measured along section DE under the different flow conditions. The analytical solution can be used (i) to reproduce each thermal response curve and (ii) to reproduce the temperature evolution measured with an external probe (PT100 no. 2; see Figure 2) located 5 cm downstream of section DE during the third heating period ($q = 1.11 \times 10^{-5}$ m/s). (c) By fixing $\lambda = 2.9$ W/m/K and $\Delta T_{FO} = 9.5°C$, the theoretical curve $\Delta T = f(q)$, at $t = 4$ h of heating, can be defined, allowing the direct association of a value of ΔT with a value of flux. MILS, Moving Instantaneous Line Source.

Figure 10b shows the application of the MILS model (Equation 7a) to reproduce the thermal response under the different flow conditions. For each case, the model was applied for $t > t_c$, when the temperature increase is fully independent of the effect of the FO cable. Modeled curves fit very well with the experimental curves. The RMSE calculated between observed data and the analytical model varies between 0.03 and 0.06°C. To validate the MILS model, the rise in temperature monitored inside the sandbox 5 cm from section DE was also modeled using the MILS model. At a 5-cm distance from the FO cable, the temperature increased by 1.75°C after a 5-min-delay, corresponding to the time required for the advective transport of heat from the heated FO cable to the probe. As shown in Figure 10b, this temperature increase can be very well reproduced using the analytical solution knowing the distance between the FO cable and the probe and considering $\lambda = 2.96$ W/m/K and $q = 1.11 \times 10^{-5}$ m/s. This result validates the use of the analytical solution and strengthens the estimate of flux.

Lastly, as shown in Figure 10c, the modeled ΔT after a given heating period ($t = 4$ h) can be calculated as a function of flux by summing the effect of the cable ΔT_{FO}, graphically determined, with the temperature increase induced by heat transfer through the porous media ΔT_{PM}, estimated using the MILS model. Experimental data points have been reported on this curve and perfectly fit on the curve obtained from the MILS model, thus providing another validation of the applicability of the proposed interpretation method based on the MILS model. The value of ΔT (at $t = 4$ h) can thus directly be used to estimate fluxes ranging

between 8×10^{-6} and 3×10^{-2} m/s. An experimental error of 0.2°C (when estimating the value ΔT_{FO} or associated with noise measurement) would induce an error of only 10% on the estimated flux. Compared to typical uncertainties associated with the estimation of hydraulic conductivity, the proposed interpretation method of active-DTS experiments provides a much better estimate of groundwater flux (Darcy velocity), with a very low uncertainty.

4. Discussion

Many active-DTS experiments were previously conducted in different reservoirs (soil, sediments, aquifer, etc.) to estimate groundwater flux and/or thermal conductivity. Here, we provide a theoretical and general framework to interpret the thermal response during active-DTS experiments. Our study contributes to a better understanding of the different thermal regimes controlling the thermal response and in particular the respective role of thermal conduction and groundwater advection. Moreover, it shows very well that the temperature increase during the early times of the experiment is simultaneously controlled by heat transfer processes occurring through both the FO cable and thermal conduction in the porous media. To go further, we clearly highlighted the role of the different parameters in the different thermal regimes. Transitional behaviors were also precisely described improving the interpretation of experimental data.

As expected, the method proposed by Des Tombes et al. (2019), also based on the MILS model, is not directly applicable when using a single heated FO cable. Indeed, the early times of ΔT_{PM} ($t < t_c$) cannot entirely be reproduced using the MILS model since heat transfer processes through the FO cable also control the temperature increase during this period. However, once ΔT_{FO} is estimated, the analytical solution can be applied starting from $t = 0$ (start of the heat injection), since heat transfer through the FO cable does not delay the thermal response (the analytical solution considering the distance from the heat source). This implies that, for $t > t_c$, the variations of temperature are similar regardless the configuration of the setup (single cable or separated heat source/FO cable) are equal to ΔT_{PM} and can consequently be reproduced using the MILS model.

The improved and full understanding of the different thermal regimes controlling the temperature increase over time led us to propose two independent and complementary methods to interpret the thermal response, each providing an independent estimate of both thermal conductivity and groundwater flux. In addition, the first method that relies on the use of the MILS model considers the temperature increase induced by the FO cable allowing its quantification. The second method that depends on three complementary characteristic times is simple to apply and has the advantage to well define the limits of the different thermal regimes. Although both methods are complementary, the use of the MILS model is certainly more convenient to estimate the distribution of groundwater flows along a FO cable. The graphical approach requires a thorough analysis of the temperature evolution. The automated estimation of the characteristic times does not seem conceivable considering data noise, meaning that a "point-by-point" analysis is required. However, the graphical approach may be used to confirm some of the results obtained with the MILS model.

Both interpretation methods were successfully tested through numerical simulations and fully validated thanks to experimental data. The approach provides estimates of the thermal conductivity and the groundwater flux with an excellent and unprecedented accuracy. Experimental results show indeed that thermal conductivity can be easily estimated with a good accuracy around 0.1–0.2 W/m/K, which corresponds to ±2.5%–10% for typical values of thermal conductivity. This accuracy depends on the quality of data and groundwater flux but is as good as or better than estimates from Heat Pulse Probes or TRTs (He, Dyck, Horton, Li, et al., 2018; He, Dyck, Horton, Ren, et al., 2018; Raymond et al. 2011). The accuracy of groundwater flux estimates is even better since our experimental results suggest it can reach a few percent which is much better than the one obtained with hydraulic methods (de Marsily, 1976). Moreover, while hydraulic methods provide in general an integrated value of hydraulic conductivity, active-DTS experiments can provide continuous groundwater flow measurements with an excellent spatial resolution close to 1 m or less (Simon et al., 2020).

In the following sections, we discuss the sensitivity of the method to the different parameters and the applicability of active-DTS experiments in the field. This provides some guidelines for users to achieve active-DTS experiments in different contexts.
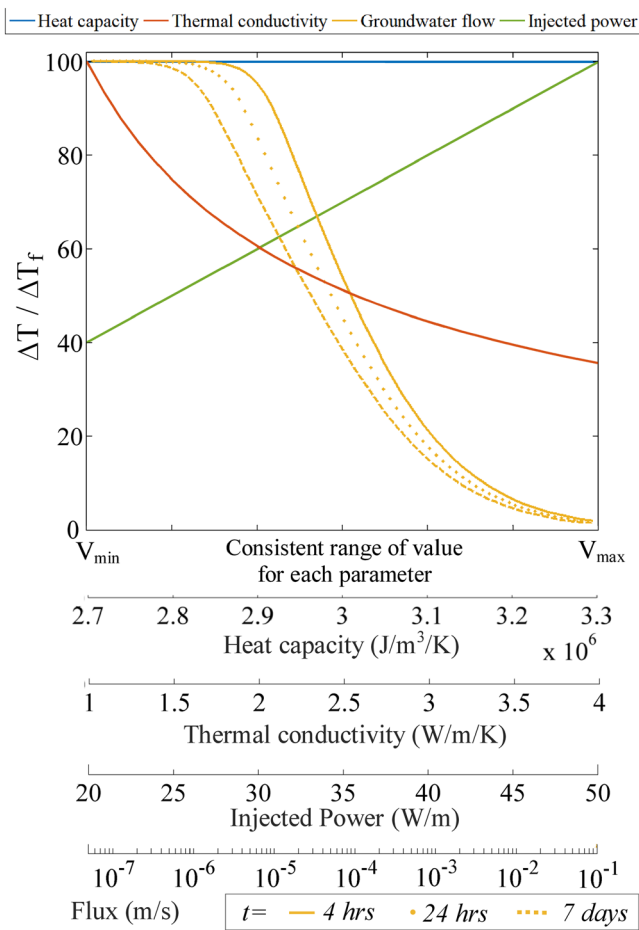
Figure 11. Sensitivity of the thermal response to the different parameters. For each parameter, the thermal response was calculated with the MILS model by fixing parameters to reference values ($Q = 35$ W/m; $\lambda = 1.4$ W/m/K; $C = 3 \times 10^6$ J/m^3/K; $q = 2 \times 10^{-5}$ m/s, and $t = 4$ h) and by varying one of the parameters over a realistic range. The dotted and dashed yellow curves correspond respectively to heating periods of 24 h and 7 days. MILS, Moving Instantaneous Line Source.

4.1. Sensitivity of Parameters on the Temperature Rise

The value of ΔT_f depends on the intensity of the injected electrical power, on porous media thermal properties and groundwater flux. Figure 11 shows the dependence of the thermal response for the different parameters. For each tested parameter, the thermal response was modeled by varying its value over a large range (see the horizontal axis of the plot) while all other parameters were fixed. ΔT_f was estimated for each simulation and then normalized relative to the higher value of ΔT_f obtained over the tested range.

The increase of temperature linearly depends on the intensity of the injected electrical power through the steel armoring of the cable, Q (W/m) (Equation 7) (see the green line in Figure 11). For a given temperature accuracy, the method should therefore be more sensitive to flow when larger values of injected electrical power are used. Variations of heat capacity (blue line) have a minimal impact on the value of ΔT_f. This is probably due to the range in heat capacity that is relatively small compared to other parameters. However, the sensitivity to thermal conductivity is greater (orange line). A strong negative and monotonic relationship exists between the thermal conductivity and the value of ΔT_f. The value of thermal conductivity highly influences the value of ΔT, since ΔT_f varies by 40% over the tested range of thermal conductivity. This confirms that the thermal conductivity directly controls the amplitude of ΔT that could be investigated as previously shown in Figure 7. This amplitude reaches almost 16°C when $\lambda = 1.1$ W/m/K but is really limited for higher values of thermal conductivity (less than 5°C for $\lambda = 4$ W/m/K). The method is therefore less sensitive to flow for larger value of thermal conductivity.

The groundwater flux has also a strong impact on the thermal response (yellow lines). Differences of ΔT are significant in a restricted range of fluxes depending on heating duration. Our results show that groundwater flux could be potentially estimated over more than 3 orders of magnitude from 2×10^{-6} to 5×10^{-2} m/s for a heating duration of $t = 4$ h (solid line). The larger the heating duration, the greater the range of fluxes that could be estimated. This improvement is especially sensitive for very low groundwater flows. Thus, the limit of detection could be as low as 1×10^{-6} m/s and even 3×10^{-7} m/s for heating durations of $t = 24$ h (dotted line) and $t = 7$ days (dashed line), respectively.

Covarying the flux and the thermal conductivity allows defining more precisely the effect of the value of thermal conductivity on q_{min} and q_{max}, beyond which the temperature increase is no more affected by flow variations. Although results are not shown, only q_{min} slightly depends on thermal conductivity. Thus, while $q_{min} \approx 1 \times 10^{-6}$ m/s for any $\lambda < 1.7$ W/m/K, the value of q_{min} slowly increases with the increase of λ and reaches 2.5×10^{-6} m/s for $\lambda = 4$ W/m/K. However, varying λ does not significantly affect the value of q_{max}.

This large measurement range (typically between 0.05 m/day to values greater than 10^2 m/day) corresponds very well to the expected groundwater flux range that should occur in natural permeable porous media (de Marsily, 1976). Thus, the active-DTS method could be appropriate for a large number of applications. Note that the limitations and the resolution of the method are similar independently of the choice of the configuration of the experiment, namely a single heated FO cable or using an external heat source as proposed by Des Tombes et al. (2019).

4.2. Uncertainty on Flux Estimates

The measurement noise in temperature measurements can induce errors when interpreting the thermal response and consequently errors on flux estimates. As suggested by results presented in Figure 4, a fixed
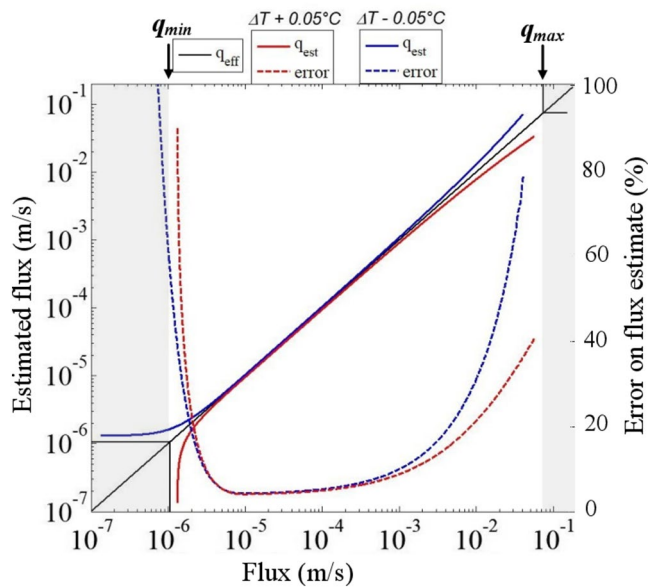
Figure 12. An error of ±0.05°C on temperature measurements results in errors on flux estimates depending on the value of the flux. The blue and red solid lines correspond to the flux estimates considering value of ΔT, respectively, equal to $\Delta T - 0.05°C$ and $\Delta T + 0.05°C$ (for $Q = 20$ W/m, $\lambda = 2.5$ W/m/K, and $t = 24$ h). The dotted lines correspond to the resulting errors on flux estimates (%).

error on temperature measurements will result in larger errors on flux estimates close to the limits q_{min} and q_{max}. The error on flux estimates associated with an error of $\pm 0.05°C$ (considering a random noise 0.1°C) was calculated and is shown in Figure 12. It appears that, between 3.94×10^{-6} and 3.6×10^{-4} m/s, an error on $\pm 0.05°C$ leads to errors on flux estimates lower than 7%. Beyond and below these values, the error increases exponentially when q tends toward the limits q_{min} and q_{max}. For instance, an error of $-0.05°C$ would induce an error of around 70% on flux estimate for $q = 9.2 \times 10^{-7}$ m/s and would lead to an estimation of the flux around 1.57×10^{-6} m/s. Note also that lower values of thermal conductivity would lead to lower errors (for a fixed temperature). Thus, for $q = 5.2 \times 10^{-5}$ m/s, the errors on flux estimates resulting from an error of $\pm 0.05°C$ would be around 2.1% for $\lambda = 1$ W/m/K, around 4.5% for $\lambda = 2.5$ W/m/K, and 6.8% for $\lambda = 4$ W/m/K. Finally, the error depends also on the injected power, since it directly controls the amplitude of the temperature increase. Thus, for instance, while the error for $q = 1 \times 10^{-5}$ m/s is around 2.4% for $Q = 35$ W/m, this value would reach 5.4% for $Q = 15$ W/m.

Therefore, the data noise can strongly decrease the accuracy on the flux estimates. The data noise depends on the DTS unit and can be reduced by increasing the measurement time, since the standard deviation of the measurement errors reduces with the square root of time (J. S. Selker, van de Giesen, et al., 2006). However, increasing the integration time affects the possibility of measuring temperature changes at the early times of the heating period, increasing errors on ΔT_{FO} and λ estimates. When the data are too noisy, the integration time can be increased for later times of the heating, which improves the estimation of ΔT_f. The temperature increase can also be filtered, for instance following the methodology proposed by Ramos et al. (2017).

4.3. Heating Durations and Applicability of the Method

The numerical model and the validated interpretation methods are used here to define the experimental conditions required to successfully apply the active-DTS method in the field. Contrary to active-DTS experiments conducted in unsaturated soils, that only require a few minutes of heating to investigate the thermal properties of the soil (Sayde et al., 2010), the application of the method for saturated conditions requires much longer heating periods, since advective heat transfers control heat propagation at later times.

The experimental duration is directly dependent on flow and can thus be related to hydraulic gradient and hydraulic conductivity. Figure 13a shows the domain of fluxes that can be investigated according to the duration of the heating period. We consider here the duration required to reach the limit between the conduction-dominant and the advection-dominant periods (t_d). As expected, the lower the flux, the longer is this duration. For instance, 4 h of heating would be required to reach t_d for fluxes equal to 2.6×10^{-6} m/s (purple line in Figure 13a). However, the temperature would be stabilized ≈12 h later, since $t_s \approx 4.28 t_d$. A 24-h heating period is required to reach the limit between conduction and advection for a flux of 1×10^{-6} m/s (light blue line). Nevertheless, the range of fluxes that can be investigated is remarkably large and 12 h of heating should be enough to investigate flows in aquifers under natural hydraulic gradient or under gradients due to pumping. Thus, the method seems very appropriate for measuring fluxes for most values of hydraulic conductivity commonly encountered in aquifers used for water resources (de Marsily, 1976).

Likewise, Figure 13b shows the heating duration required to reach characteristic times t_s and t_d according to groundwater flux. Typically, 12 h of heating are enough to investigate a flux larger than 0.5 m/day. For low fluxes ($<7 \times 10^{-7}$ m/s), the thermal response would be similar to the thermal response under no flow (no temperature stabilization) even for very long heating durations. Thus, in practice, measurements of fluxes lower than 10^{-17} m/s appear very difficult to achieve. It should be noted that stabilization is not necessarily
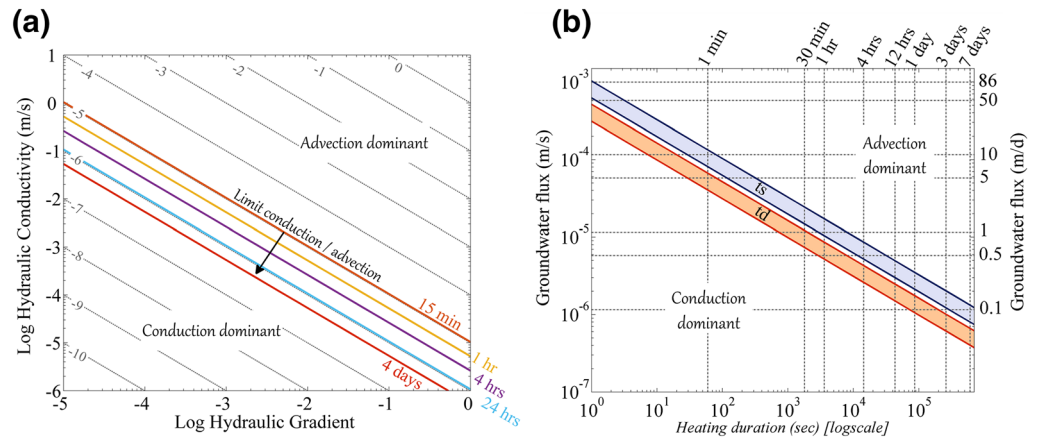
Figure 13. (a) Duration of the heating period required to reach the characteristic time t_d that marks the limit between the conduction-dominant period and the advection-dominant period for a large range of hydraulic gradients and hydraulic conductivities. These results are based on the calculation of the characteristic times t_d (see Figure 6) considering $\lambda = 1.1$ W/m/K, $\rho_c = 3 \times 10^6$ J/m³/K, and $\rho_w c_w = 4.1 \times 10^6$ J/m³/K. Note that, under these conditions, $t_s \approx 4.28 t_d$, meaning that the experiment should be more than 4 times longer to reach the temperature stabilization. Each diagonal gray line corresponds to a flux value that depends on the hydraulic gradient and hydraulic conductivity. (b) Heating duration required to reach the characteristic times t_s and t_d according to the flux, considering $\rho_c = 3 \times 10^6$ J/m³/K and $\rho_w c_w = 4.1 \times 10^6$ J/m³/K and λ varying between 1.1 and 3 W/m/K.

required to estimate fluxes, since the MILS model, by reproducing the temperature evolution during the transition period before the temperature stabilization, may provide a good estimate of flux. Thus, although the uncertainty would be higher, a flux can be estimated as long as the transition period is established (slope s_2). Note that the value of the thermal conductivity also affects t_s and t_d. It appears from the results presented in Figure 13b that a change of λ from 1.1 to 3 W/m/K multiplies by 2.73 (ratio 3/1.1) the duration required to reach t_s and t_d independently of groundwater flux. For instance, for $q = 1 \times 10^{-6}$ m/s, more than 3 days of heating are required to reach the stabilization time when $\lambda = 1.1$ W/m/K while almost 9 days would be required if $\lambda = 3$ W/m/K. Therefore, the value of the thermal conductivity must be considered when applying active experiments, especially for the estimation of low groundwater flux.

4.4. Experimental Conditions to Apply the Method

Considering the experimental setup, and especially the continuous injection of electricity, it may still be difficult to ensure experiments that would exceed more than a few days. This limitation also depends on the specific application since the measurement duration should also be shorter than hydraulic changes that may occur in the field. This may be an issue in flow systems characterized by rapid dynamics like, for instance streambeds, where hyporheic exchanges can fluctuate rapidly due to rapid stream stage fluctuations induced by dam operations, floods, or snowmelt (Ferencz et al., 2019; Gerecht et al., 2011; Gomez-Velez et al., 2017; Hucks Sawyer et al., 2009; Singh et al., 2019). Thus, although the active-DTS method may also be used to monitor groundwater flows, a possible limitation may arise from the duration required for such measurements, which may exceed the groundwater dynamics variability of some flow systems.

Concerning the power supply, the method requires the perfect control of the heat injection. Injecting a constant and reliable electrical current can be difficult since the resistance of the FO cable (plastic and steel core) depends on the temperature of the wire. This challenge was overcome through the use of a reliable power controller that continuously measures the resistance of the electrical circuit including both FO and electrical cables. It therefore adjusts the input voltage and intensity in the circuit, to ensure injecting a constant electrical power Q. We suggest injecting an electrical power between 15 and 35 W/m, that is high enough to improve the resolution of measurements and to decrease errors on flux estimates (the higher the electrical power, the larger the range of ΔT measured). However, consistent results could also be obtained with lower values of Q (up to 5 W/m), even though the associated estimates of fluxes would be less accurate. It can offer the possibility of heating longer sections of cable (for the same amount of power delivered). In

any case, the selection of the injected electrical power must be made carefully according to the length of the heated section, the desired temperature increase, and safety issues.

To reduce the resistance of the electrical circuit and thus the supply of electricity, we recommend using cooper electrical cables having large cable sections, associated with lower values of resistivity. For instance, we used a 6-mm^2 cable section whose resistance is around 2.92 Ω/km. The selection of the FO cable depends on its thermal conductivity that should be high enough to ensure a fast thermal response.

The thermal properties of soils depend also on temperature (Hopmans & Dane, 1986; Sepaskhah & Boersma, 1979). The temperature increase in sediments could thus induce errors on thermal conductivity estimates. However, it has been shown that temperature increase does not significantly modify the thermal properties of sands below 50°C for fully saturated conditions (Smits et al., 2013). Here, the effect of the increase of temperature on the thermal properties of the media could therefore be assumed as negligible if the injected electrical power is low enough to maintain the sediments temperature inferior to 50°C. Likewise, lower temperature increases ensure that free natural convection remains negligible despite the temperature gradient induced by heat injection. Calculation of the Rayleigh–Darcy number to estimate the possible occurrence of convective effects (Nield & Bejan, 2013) confirms that free thermal convection should be negligible in the present case. However, free convection may dominate transport processes for gravel characterized by a large average grain size and a very high permeability. Note also that the stability of the background temperature may be an important issue to be able to interpret correctly the data, especially in the very shallow subsurface. Wu et al. (2019) also noted that the repetition of heated tests requires accounting for hysteresis effects caused by repeated heating and recovery cycles that induce the difficulty for the porous media to return to its initial ambient temperature.

Finally, it should be noted that active-DTS methods remain invasive and that the installation of the FO cable can lead to the sediment disturbance that can potentially affects the values of both the thermal properties and the groundwater flux. The cables, including both FO and electrical cables, can be efficiently buried with direct-push equipment, just as described by Bakker et al. (2015). Nevertheless, it is clear that direct-push methods can be used only in sandy or granular aquifers, which may be a major limitation to apply the method. The in-stream installation of FO cables for instance could require using some tools, like plows, to limit the alteration of the riverbed and to control the burial depth of the cable. Lastly, the question of the installation of the FO cable indirectly raises the question of the flow direction in relation to the FO cable. Although results are not shown here, temperature increases measured along the sections EF and FG during sandbox experiments allow highlighting that the angle of the flow with the FO cable could affect the thermal response. These results will be the subject of an upcoming study.

5. Conclusions

This study provides a full framework allowing the generalization of the application of active-DTS methods in the field to characterize flows in saturated porous media. The methodology relies on the interpretation of the thermal response occurring along a single heated FO cable used both for injecting heat and for recording temperature changes. The combination of a numerical model with laboratory experiments allowed (i) improving the understanding of the thermal processes controlling the temperature increase, (ii) fully validating two complementary and independent interpretation methods providing an estimate of both the thermal conductivity and the groundwater flux, and (iii) defining the limits of the measurements of the method and discuss its applicability in the field. More specifically, the following conclusions can be drawn:

(1) By delimiting the duration of the conduction-dominant stage, the effective thermal conductivity of the media can easily be estimated independently of groundwater flow (i) by graphically estimating the slope of the temperature increase during this stage and (ii) by reproducing the temperature rise using the MILS model considering no-flow conditions. Thus, the approach proposed provides two simple independent estimates of thermal conductivity, thus reducing the uncertainty of the estimation. From our experimental results, the error associated with thermal conductivity estimates ranges between ±0.2 and ±0.4 W/m/K. Thus, active-DTS experiments can provide the spatial variability of the thermal conductivity in the field, which can be very useful, especially for geothermal applications.

(2) Although the FO cable has a clear and significant effect on the thermal response during the very early times of active-DTS experiments, this effect can easily be graphically defined and delimited in time. The temperature evolution induced by heat transfer occurring in the porous media can then be modeled efficiently using the MILS analytical solution to provide accurate estimates of groundwater fluxes.

(3) The graphical analysis of the thermal response curves obtained along the cable can also provide an accurate and independent estimation of flux by defining three characteristic times t_d, t_i, and t_s. Although the graphical determination of these times can be coarse because of the log-time scale or noise in the data, the three characteristic times can provide complementary results that can greatly help to identify a representative value of flux. The main advantage of this approach is that its application is independent of the effect of the FO cable.

(4) The characterization of both the FO cable effect and the validation of the MILS model allows the prediction of the increase in temperature after a given heating time for a given flux and thermal conductivity. The MILS thus provides a theoretical curve relating the thermal response of the porous media to flux q for a given thermal conductivity λ after a specific heating time t: $\Delta T_{PM} = f(q, \lambda, t)$. With this function, values of temperature rise ΔT_{PM} can be directly related to their corresponding fluxes allowing the rapid and accurate conversion of active-DTS temperature measurements into flux estimates

We showed that active-DTS experiments allow the estimation of groundwater fluxes varying between 3×10^{-6} and 5×10^{-2} m/s (for a heating duration of 4 h) and that the limit of detection could be as low as 1×10^{-6} m/s after 24 h of heating. The active-DTS method could thus be potentially applied to a very wide range of flow systems having fluxes within the more than 3 orders of magnitude of measurable flux values. In the field, the reliable and direct estimation of the distribution of fluxes could replace the measurement of hydraulic conductivity, whose distribution and variability still remains difficult and time consuming to evaluate in the field.

Finally, this method could address the challenge of characterizing the distribution of fluxes in the subsurface. Depending on the spatial resolution of the DTS units and on experimental conditions (Simon et al., 2020), the method can provide flux estimates all along a FO cable at a very high sampling resolution that is not reachable with other conventional methods. This results in the possibility of precisely mapping heterogeneities and understanding flow dynamics, such as for instance in sandy aquifers or in the hyporheic zone, where the spatial distribution of flow can be driven by very local heterogeneities (Cardenas, 2015). This opens the possibility of applying active-DTS method for a wide range of applications where the variability of groundwater flows is critical, such as groundwater/surface water interactions, contaminant transport, and for safety and technical issues such as leaks in levees or the efficiency of geothermal systems.

Data Availability Statement

The data presented in this paper are available and accessible through the following link at database of the H+ French National Network for Hydrogeological sites: http://hplus.ore.fr/en/simon-et-al-2020-wrr-data

References

Anderson, M. P. (2005). Heat as a ground water tracer. *Ground Water*, *43*(6), 951–968. https://doi.org/10.1111/j.1745-6584.2005.00052.x

Aufleger, M., Conrad, M., Goltz, M., Perzlmaier, S., & Porras, P. (2007). Innovative dam monitoring tools based on distributed temperature measurement. *Jordan Journal of Civil Engineering*, *1*, 29–37.

Bakker, M., Calje, R., Schaars, F., van der Made, K.-J., & de Haas, S. (2015). An active heat tracer experiment to determine groundwater velocities using fiber optic cables installed with direct push equipment. *Water Resources Research*, *51*, 2760–2772. https://doi.org/10.1002/2014WR016632

Bakx, W., Doornenbal, P. J., Van Weesep, R. J., Bense, V. F., Oude Essink, G H. P., & Bierkens, M. F. P. (2019). Determining the relation between groundwater flow velocities and measured temperature differences using active heating-distributed temperature sensing. *Water*, *11*, 1619. https://doi.org/10.3390/w11081619

Banks, E. W., Shanafield, M. A., & Cook, P. G. (2014). Induced Temperature Gradients to Examine Groundwater Flowpaths in Open Boreholes. *Groundwater*, *52*(6), 943–951. https://doi.org/10.1111/gwat.12157

Benítez-Buelga, J., Sayde, C., Rodríguez-Sinobas, L., & Selker, J. S. (2014). Heated Fiber Optic Distributed Temperature Sensing: A Dual-Probe Heat-Pulse Approach. *Vadose Zone Journal*, *13*(11), vzj2014.02.0014. https://doi.org/10.2136/vzj2014.02.0014

Bense, V. F., Read, T., Bour, O., Le Borgne, T., Coleman, T., & Krause, S., et al. (2016). Distributed temperature sensing as a downhole tool in hydrogeology. *Water Resources Research*, *52*, 9259–9273. https://doi.org/10.1002/2016WR018869

Blackwell, J. H. (1954). A Transient-Flow Method for Determination of Thermal Constants of Insulating Materials in Bulk Part I—Theory. *Journal of Applied Physics*, *25*(2), 137–144. https://doi.org/10.1063/1.1721592

Cardenas, M. B. (2015). Hyporheic zone hydrologic science: A historical account of its emergence and a prospectus. *Water Resources Research*, *51*, 3601–3616. https://doi.org/10.1002/2015WR017028

Carslaw, H. S., & Jaeger, J. C. (1959). *Conduction of heat in solids*, Oxford, UK: Oxford University Press. https://infoscience.epfl.ch/record/27427

Coleman, T. I., Parker, B. L., Maldaner, C. H., & Mondanos, M. J. (2015). Groundwater flow characterization in a fractured bedrock aquifer using active DTS tests in sealed boreholes. *Journal of Hydrology*, *528*, 449–462. https://doi.org/10.1016/j.jhydrol.2015.06.061

Del Val, L. (2020). *Advancing in the characterization of coastal aquifers. A multimethodological approach based on fiber optics distributed temperature sensing*, Barcelona, Spain: (PhD thesis). Universitat Politècnica de Catalunya.

des Tombe, B. F., Bakker, M., Smits, F., Schaars, F., & van der Made, K.-J. (2019). Estimation of the variation in specific discharge over large depth using distributed temperature sensing (DTS) measurements of the heat Pulse response. *Water Resources Research*, *55*, 811–826. https://doi.org/10.1029/2018WR024171

Diao, N., Li, Q., & Fang, Z. (2004). Heat transfer in ground heat exchangers with groundwater advection. *International Journal of Thermal Sciences*, *43*(12), 1203–1211. https://doi.org/10.1016/j.ijthermalsci.2004.04.009

Domenico, P. A., & Schwartz, F. W. (1998). *Physical and chemical hydrogeology* (2nd ed.). New York: John Wiley & Sons Inc).

Ferencz, S. B., Cardenas, M. B., & Neilson, B. T. (2019). Analysis of the effects of dam release properties and ambient groundwater flow on surface water-groundwater exchange over a 100-km-long reach. *Water Resources Research*, *55*, 8526–8546. https://doi.org/10.1029/2019WR025210

Foster, M., Fell, R., & Spannagle, M. (2000). The statistics of embankment dam failures and accidents. *Canadian Geotechnical Journal*, *37*(5), 1000–1024. https://doi.org/10.1139/t00-030

Freeze, R., & Cherry, J. (1979). *GroundWater* (Vol. 16, pp. 1–604, 1 ed). London, UK: Pearson.

Gerecht, K. E., Cardenas, M. B., Guswa, A. J., Sawyer, A. H., Nowinski, J. D., & Swanson, T. E. (2011). Dynamics of hyporheic flow and heat transport across a bed-to-bank continuum in a large regulated river. *Water Resources Research*, *47*, W03524. https://doi.org/10.1029/2010WR009794

Freifeld, B. M., Finsterle, S., Onstott, T. C., Toole, P., & Pratt, L. M. (2008). Ground surface temperature reconstructions: Using in situ estimates for thermal conductivity acquired with a fiber-optic distributed thermal perturbation sensor. *Geophysical Research Letters*, *35*(14), L14309–14313. https://doi.org/10.1029/2008gl034762

Gomez-Velez, J. D., Wilson, J. L., Cardenas, M. B., & Harvey, J. W. (2017). Flow and residence times of dynamic river bank storage and sinuosity-driven hyporheic exchange. *Water Resources Research*, *53*, 8572–8595. https://doi.org/10.1002/2017WR021362

Habel, W., Baumann, I., Berghmans, F., Borzycki, K., Chojetzki, C., Haase, K.-H., et al. (2009). *Guideline for use of fiber optic sensors*, (–). Brussels, Belgium: COST.

Hantush, M. S. (1956). Analysis of data from pumping tests in leaky aquifers. *Transactions: American Geophysical Union*, *37*(6), 702. https://doi.org/10.1029/TR037i006p00702

Hantush, M. S., & Jacob, C. E. (1955). Non-steady radial flow in an infinite leaky aquifer. *Transactions: American Geophysical Union*, *36*(1), 95. https://doi.org/10.1029/TR036i001p00095

He, H., Dyck, M. F., Horton, R., Li, M., Jin, H., & Si, B. (2018). Chapter five—Distributed temperature sensing for soil physical measurements and its similarity to heat Pulse method. In D. L. Sparks (Ed.), Advances in agronomy (Vol. 148, pp. 173–230). Cambridge, MA: Academic Press. https://doi.org/10.1016/bs.agron.2017.11.003

He, H., Dyck, M. F., Horton, R., Ren, T., Bristow, K. L., Lv, J., & Si, B. (2018). Development and application of the heat Pulse method for soil physical measurements. *Reviews of Geophysics*, *56*, 567–620. https://doi.org/10.1029/2017RG000584

Hopmans, J. W., & Dane, J. H. (1986). Thermal conductivity of two porous media as a function of water content, temperature, and density. *Soil Science*, *142*(4), 187–195. https://doi.org/10.1097/00010694-198610000-00001

Hucks Sawyer, A., Bayani Cardenas, M., Bomar, A., & Mackey, M. (2009). Impact of dam operations on hyporheic exchange in the riparian zone of a regulated river. *Hydrological Processes*, *23*(15), 2129–2137. https://doi.org/10.1002/hyp.7324

Kalbus, E., Reinstorf, F., & Schirmer, M. (2006). Measuring methods for groundwater–surface water interactions: A review. *Hydrology and Earth System Sciences*, *10*(6), 873–887.

Kalbus, E., Schmidt, C., Molson, J. W., Reinstorf, F., & Schirmer, M. (2009). Influence of aquifer and streambed heterogeneity on the distribution of groundwater discharge. *Hydrology and Earth System Sciences*, *13*(1), 69–77.

Kurylyk, B. L., & Irvine, D. J. (2019). Heat: An overlooked tool in the practicing hydrogeologist's toolbox. *Groundwater*, *57*(4), 517–524. https://doi.org/10.1111/gwat.12910

Kurylyk, B. L., Irvine, D. J., & Bense, V. F. (2019). Theory, tools, and multidisciplinary applications for tracing groundwater fluxes from temperature profiles. *Wiley Interdisciplinary Reviews: Water*, *6*(1), e1329. https://doi.org/10.1002/wat2.1329

Leaf, A. T., Hart, D. J., & Bahr, J. M. (2012). Active thermal tracer tests for improved hydrostratigraphic characterization. *Groundwater*, *50*(5), 726–735. https://doi.org/10.1111/j.1745-6584.2012.00913.x

Liu, G., Knobbe, S., & Butler, J. J., Jr. (2013). Resolving centimeter-scale flows in aquifers and their hydrostratigraphic controls. *Geophysical Research Letters*, *40*, 1098–1103. https://doi.org/10.1002/grl.50282

Maldaner, C. H., Munn, J. D., Coleman, T. I., Molson, J. W., & Parker, B. L. (2019). Groundwater flow quantification in fractured rock boreholes using active distributed temperature sensing under natural gradient conditions. *Water Resources Research*, *55*, 3285–3306. https://doi.org/10.1029/2018WR024319

Mao, D., Yeh, T.-C. J., Wan, L., Hsu, K.-C., Lee, C.-H., & Wen, J.-C. (2013). Necessary conditions for inverse modeling of flow through variably saturated porous media. *Advances in Water Resources*, *52*, 50–61. https://doi.org/10.1016/j.advwatres.2012.08.001

de Marsily, G. (1976). *Cours d'hydrogéologie*, Paris, France: Ecole Nationale Supérieure des Mines de Paris, Centre d'Informatique géologique.

Metzger, T., Didierjean, S., & Maillet, D. (2004). Optimal experimental estimation of thermal dispersion coefficients in porous media. *International Journal of Heat and Mass Transfer*, *47*(14–16), 3341–3353. https://doi.org/10.1016/j.ijheatmasstransfer.2004.02.024

Molina-Giraldo, N., Bayer, P., & Blum, P. (2011). Evaluating the influence of thermal dispersion on temperature plumes from geothermal systems using analytical solutions. *International Journal of Thermal Sciences*, *50*(7), 1223–1231. https://doi.org/10.1016/j.ijthermalsci.2011.02.004

COMSOL Multiphysics. (2019). Introduction to COMSOL multiphysics. Version 5.5. COMSOL. Burlington, MA.

Munn, J. D., Maldaner, C. H., Coleman, T. I., & Parker, B. L. (2020). Measuring fracture flow changes in a bedrock aquifer due to open hole and pumped conditions using active distributed temperature sensing. *Water Resources Research*, *56*, e2020WR027229. https://doi.org/10.1029/2020WR027229

Nield, D. A., & Bejan, A. (2013). *Convection in porous media* (4th ed.). New York, NY: Springer.

Papadopulos, I. S., & Cooper, H. H., Jr. (1967). Drawdown in a well of large diameter. *Water Resources Research*, *3*(1), 241–244. https://doi.org/10.1029/WR003i001p00241

Pehme, P. E., Parker, B. L., Cherry, J. A., & Greenhouse, J. P. (2010). Improved resolution of ambient flow through fractured rock with temperature logs. *Groundwater*, *48*(2), 191–205. https://doi.org/10.1111/j.1745-6584.2009.00639.x

Perzlmaier, S., Aufleger, M., & Conrad, M. (2004). *Distributed fiber optic temperature measurements in hydraulic engineering: Prospects of the heat-up method*. Paper presented at Proceedings of a Workshop on Dam Safety Problems and Solutions, 72nd ICOLD Annual Meeting, Seoul, South Korea.

Poeter, E., & Gaylord, D. R. (1990). Influence of aquifer heterogeneity on contaminant transport at the Hanford site. *Groundwater*, *28*(6), 900–909. https://doi.org/10.1111/j.1745-6584.1990.tb01726.x

Ramos, G., Carrera, J., Gómez, S., Minutti, C., & Camacho, R. (2017). A stable computation of log-derivatives from noisy drawdown data. *Water Resources Research*, *53*, 7904–7916. https://doi.org/10.1002/2017WR020811

Rau, G. C., Andersen, M. S., McCallum, A. M., Roshan, H., & Acworth, R. I. (2014). Heat as a tracer to quantify water flow in near-surface sediments. *Earth-Science Reviews*, *129*, 40–58. https://doi.org/10.1016/j.earscirev.2013.10.015

Raymond, J., Therrien, R., & Gosselin, L. (2011). Borehole temperature evolution during thermal response tests. *Geothermics*, *40*(1), 69–78. https://doi.org/10.1016/j.geothermics.2010.12.002

Read, T. (2016). *Applications of distributed temperature sensing in subsurface hydrology* (PhD thesis). Norwich, UK: University of East Anglia. https://ueaeprints.uea.ac.uk/59401/1/T-Read_2016_PhDThesis.pdf

Read, T., Bense, V. F., Hochreutener, R., Bour, O., Le Borgne, T., Lavenant, N., & Selker, J. S. (2015). Thermal-plume fiber optic tracking (T-POT) test for flow velocity measurement in groundwater boreholes. *Geoscientific Instrumentation, Methods and Data Systems*, *4*(2), 197–202. https://doi.org/10.5194/gi-4-197-2015

Read, T., Bour, O., Selker, J. S., Bense, V. F., Borgne, T. L., Hochreutener, R., & Lavenant, N. (2014). Active-distributed temperature sensing to continuously quantify vertical flow in boreholes. *Water Resources Research*, *50*, 3706–3713. https://doi.org/10.1002/2014WR015273

Renard, P., Glenz, D., & Mejias, M. (2008). Understanding diagnostic plots for well-test interpretation. *Hydrogeology Journal*, *17*(3), 589–600. https://doi.org/10.1007/s10040-008-0392-0

Sayde, C., Buelga, J. B., Rodriguez-Sinobas, L., El Khoury, L., English, M., van de Giesen, N., & Selker, J. S. (2014). Mapping variability of soil water content and flux across 1–1000 m scales using the Actively Heated Fiber Optic method. *Water Resources Research*, *50*, 7302–7317. https://doi.org/10.1002/2013WR014983

Sayde, C., Gregory, C., Gil-Rodriguez, M., Tufillaro, N., Tyler, S., van de Giesen, N., et al. (2010). Feasibility of soil moisture monitoring with heated fiber optics. *Water Resources Research*, *46*, W06201. https://doi.org/10.1029/2009WR007846

Sayde, C., Thomas, C. K., Wagner, J., & Selker, J. (2015). High-resolution wind speed measurements using actively heated fiber optics. *Geophysical Research Letters*, *42*, 10064–10073. https://doi.org/10.1002/2015GL066729

SEAFOM. (2010). *Measurement specification for distributed temperature sensing (SEAFOM-MSP-01)*, Epsom, UK: SEAFOM. http://www.seafom.com/

Selker, F., Selker, J. (2018). Investigating Water Movement Within and Near Wells Using Active Point Heating and Fiber Optic Distributed Temperature Sensing. *Sensors*, *18*(4), 1023–1036. https://doi.org/10.3390/s18041023

Selker, J. S., Thevenaz, L., Huwald, H., Mallet, A., Luxemburg, W., van de Giesen, N., et al. (2006). Distributed fiber-optic temperature sensing for hydrologic systems. *Water Resources Research*, *42*, W12202. https://doi.org/10.1029/2006WR005326

Selker, J. S., van de Giesen, N., Westhoff, M., Luxemburg, W., & Parlange, M. B. (2006). Fiber optics opens window on stream dynamics. *Geophysical Research Letters*, *33*, L24401. https://doi.org/10.1029/2006GL027979

Sepaskhah, A. R., & Boersma, L. (1979). Thermal conductivity of soils as a function of temperature and water Content. *Soil Science Society of America Journal*, *43*(3), 439–444. https://doi.org/10.2136/sssaj1979.03615995004300030003x

Shanafield, M., Banks, E. W., Arkwright, J. W., & Hausner, M. B. (2018). Fiber-optic sensing for environmental applications: Where we have come from and what is possible. *Water Resources Research*, *54*, 8552–8557. https://doi.org/10.1029/2018WR022768

Simon, N., Bour, O., Lavenant, N., Porel, G., Nauleau, B., Pouladi, B., & Longuevergne, L. (2020). A Comparison of Different Methods to Estimate the Effective Spatial Resolution of FO-DTS Measurements Achieved during Sandbox Experiments. *Sensors*, *20*(2), 570–591. https://doi.org/10.3390/s20020570

Singh, T., Wu, L., Gomez-Velez, J. D., Lewandowski, J., Hannah, D. M., & Krause, S. (2019). Dynamic hyporheic zones: Exploring the role of peak flow events on bedform-induced hyporheic exchange. *Water Resources Research*, *55*, 218–235. https://doi.org/10.1029/2018WR022993

Smits, K. M., Sakaki, T., Howington, S. E., Peters, J. F., & Illangasekare, T. H. (2013). Temperature Dependence of Thermal Properties of Sands across a Wide Range of Temperatures (30-70°C). *Vadose Zone Journal*, *12*(1), vzj2012.0033. https://doi.org/10.2136/vzj2012.0033

Smolen, J. J., & van der Spek, A. (2003). *Distributed temperature sensing—A DTS primer for oil & gas production. Tech. Report, Shell*. The Hague, The Netherlands: Shell International Exploration and Production.

Sophocleous, M. (2002). Interactions between groundwater and surface water: The state of the science. *Hydrogeology Journal*, *10*(1), 52–67. https://doi.org/10.1007/s10040-001-0170-8

Stallman, R. W. (1965). Steady one-dimensional fluid flow in a semi-infinite porous medium with sinusoidal surface temperature. *Journal of Geophysical Research*, *70*(12), 2821–2827. https://doi.org/10.1029/jz070i012p02821

Stauffer, F., Bayer, P., Blum, P., Molina Giraldo, N., & Kinzelbach, W. (2013). *Thermal use of shallow groundwater*. (1st Ed., pp. 287). Boca Raton, Florida: CRC Press. https://doi.org/10.1201/b16239

Sutton, M., Nutter, D., & Couvillion, R. (2003). A ground resistance for vertical bore heat exchangers with groundwater flow. *Journal of Energy Resources Technology*, *125*, 183–189. https://doi.org/10.1151/1.1591203

Tyler, S. W., Selker, J. S., Hausner, M. B., Hatch, C. E., Torgersen, T., Thodal, C. E., & Schladow, S. G. (2009). Environmental temperature sensing using Raman spectra DTS fiber-optic methods. *Water Resources Research*, *45*, W00D23. https://doi.org/10.1029/2008WR007052

Ukil, A., Braendle, H., & Krippner, P. (2012). Distributed temperature sensing: Review of technology and applications. *IEEE Sensors Journal: IEEE SENS J*, *12*, 885–892. https://doi.org/10.1109/JSEN.2011.2162060

van de Giesen, N., Steele-Dunne, S. C., Jansen, J., Hoes, O., Hausner, M. B., Tyler, S., & Selker, J. (2012). Double-ended calibration of fiber-optic Raman spectra distributed temperature sensing data. *Sensors*, *12*(5), 5471–5485. https://doi.org/10.3390/s120505471

Vélez Márquez, M., Raymond, J., Blessent, D., Philippe, M., Simon, N., Bour O., & Lamarche, L. (2018). Distributed Thermal Response Tests Using a Heating Cable and Fiber Optic Temperature Sensing. *Energies*, *11*(11), 3059–3082. https://doi.org/10.3390/en11113059

Weiss, J. D. (2003). Using fiber optics to detect moisture intrusion into a landfill cap consisting of a vegetative soil barrier. *Journal of the Air & Waste Management Association*, *53*(9), 1130–1148. https://doi.org/10.1080/10473289.2003.10466268

Wu, R., Martin, V., McKenzie, J., Broda, S., Bussière, B., Aubertin, M., & Kurylyk, B. L. (2019). Laboratory-scale assessment of a capillary barrier using fiber optic distributed temperature sensing (FO-DTS). *Canadian Geotechnical Journal*, *57*(1), 115–126. https://doi.org/10.1139/cgj-2018-0283

Zhang, B., Gu, K., Shi, B., Liu, C., Bayer, P., Wei, G., et al. (2020). Actively heated fiber optics based thermal response test: A field demonstration. *Renewable and Sustainable Energy Reviews*, *134*, 110336. https://doi.org/10.1016/j.rser.2020.110336

Zubair, S. M., & Chaudhry, M. A. (1996). Temperature solutions due to time-dependent moving-line-heat sources. *Heat and Mass Transfer*, *31*(3), 185–189. https://doi.org/10.1007/BF02333318